Inorg. Chem. **2009**, *48*, 3542−3561

Synthesis, Characterization, and Application of Vanadium−Salan Complexes in Oxygen Transfer Reactions

Pedro Adão,[†] João Costa Pessoa,*[,†] Rui T. Henriques,[†] Maxim L. Kuznetsov,[†] Fernando Avecilla,[‡] Mannar R. Maurya,[§] Umesh Kumar,[§] and Isabel Correia*[,†]

Centro de Química Estrutural, Instituto Superior Técnico, TU Lisbon, Av. Rovísco Pais, 1049-001 Lisboa, Portugal, Departamento de Química Fundamental, Universidade da Coruña, Campus de A Zapateira, 15071 A Coruña, Spain, and Department of Chemistry, Indian Institute of Technology Roorkee, Roorkee 247 667, India

Received September 19, 2008

We report the synthesis and characterization of several chiral salen- and salan-type ligands and their vanadium complexes, which are derived from salicylaldehyde or salicylaldehyde derivatives and chiral diamines (1*R*,2*R*-diaminocyclohexane, 1*S*,2*S*-diaminocyclohexane, and 1*S*,2*S*-diphenylethylenediamine). The structures of H_2sal(*R*,*R*-chan)$^{2+}\cdot 2Cl^-\cdot (CH_3)_2CHOH\cdot H_2O$ (**1c**; H_2sal(*R*,*R*-chan) = N,N′-salicyl-*R*,*R*-cyclohexanediaminium), Etvan(*S*,*S*-chen) (**3c**; Etvan(*S*,*S*-chen) = N,N′-3-ethoxy-salicylidene-*S*,*S*-cyclohexanediiminato), and naph(*R*,*R*-chen) (**6c**; naph(*R*,*R*-chen) = N,N′-naphthylidene-*R*,*R*-cyclohexanediiminato) were determined by single-crystal X-ray diffraction. The corresponding vanadium(IV) complexes and several other new complexes involving different salicylaldehyde-type precursors were prepared and characterized in the solid state and in solution by spectroscopic techniques: UV−vis, circular dichroism, electron paramagnetic resonance, and ^{51}V NMR, which provide information on the coordination geometry. The salan complexes oxidize in organic solvents to V^V species, and this process was also studied using spectroscopic techniques. Single crystals suitable for X-ray diffraction were obtained for $[\{V^VO[sal(S,S\text{-dpan})]\}_2(\mu\text{-O})]\cdot H_2O\cdot 2(CH_3)_2CHOH$ (**14c**; sal(*S*,*S*-dpan) = N,N′-salicyl-*S*,*S*-diphenylethylenediaminato) and $[\{V^VO[t\text{-Busal}(R,R\text{-chan})]\}_2(\mu\text{-O})]\cdot 2(CH_3)_2CHOH$ (**15c**), both containing an $OV^V(\mu\text{-O})V^VO$ moiety ($V_2O_3^{4+}$ core) with tetradentate ligands and one μ-oxo bridge. Both structures are the first examples of dinuclear vanadium complexes involving the $V^V_2O_3^{4+}$ core with tetradentate ligands, the configuration of the V_2O_3 unit being twist-angular. The V−salen and V−salan complexes are tested as catalysts in the oxidation of styrene, cyclohexene, cumene, and methyl phenyl sulfide with H_2O_2 and *t*-BuOOH as oxidants. Overall, the V−salan complexes show higher activity and normally better selectivity in alkene oxidation and higher activity and enantioselectivity for sulfoxidation than their parent V−salen complexes, therefore being an advantageous alternative ligand system for oxidation catalysis. The better performance of V−salan complexes probably results from their significantly higher hydrolytic stability. Mechanisms for the alkene oxidation with these newly obtained V−salan compounds are discussed, including the use of DFT for the comparison of several alternative mechanisms for epoxidation.

Introduction

Traditional methods for the oxidation of organic substrates have involved the use of stoichiometric amounts of high-valent metal compounds. These types of reactions generate large amounts of toxic waste and are becoming less popular due to growing environmental concerns. Besides being environmentally more benign, catalytic oxidations of organic compounds with oxidants such as molecular oxygen and hydrogen peroxide are less wasteful than the traditional methods and are now important reactions both in the laboratory and on an industrial scale.

Salen complexes are a standard system in coordination chemistry and have great potential as catalysts for oxo transfer reactions[1,2] and other processes.[3] One of the first uses of metal salen complexes for catalytic asymmetric

* To whom correspondence should be addressed. E-mail: joao.pessoa@ist.utl.pt (J.C.P.).
[†] TU Lisbon.
[‡] Universidade da Coruña.
[§] Indian Institute of Technology Roorkee.

10.1021/ic8017985 CCC: $40.75
Published on Web 03/16/2009

reactions was the vanadyl-catalyzed oxidation of sulfides reported by Fujita et al.[4] Later came a breakthrough with the work of Jacobsen et al.[5] and Katsuki and Kokubo,[6] who developed the enantioselective epoxidation of nonfunctionalized alkenes using chiral Mn(salen) complexes as catalysts. A wide variety of reactions catalyzed by salen complexes have been developed.[1−3] However, for the application of these reactions in the synthesis of fine chemicals, their activity, selectivity, and catalyst stability as well as their recycling ability need to be improved.

Moreover, in solution, salen ligands have the disadvantage of the hydrolysis of the C═N bond, particularly in water-containing solvents.[7,8] Reduction of the imine bonds to give an amine may present advantages. The salen-reduced derivatives (also called tetrahydrosalen and hereafter designated salan)[9] are much less studied and exhibit different structural and chemical properties: the presence of an amine backbone (instead of an imine) results in a more flexible structure, which is also more resistant to hydrolysis. Several salan complexes have been synthesized and characterized, namely, with Cu^{II},[10−13] Co^{II},[11] Ni^{II},[13,14] $V^{IV}O$,[7,8] and Zn^{II}.[15] Our group has been studying salan complexes for several years: we reported studies on the solution speciation of salan-type ligands with V(IV and V),[7,8] Cu(II),[13] Ni(II),[13] and Zn(II).[15] Our aim was to study their coordination ability and to identify species and binding modes formed in solution. Several single-crystal X-ray structures were obtained of both the ligands and the metal complexes,[7,8] and in all cases the flexibility of the ligand was evidenced. The speciation studies (by pH potentiometry and spectroscopic techniques) showed a higher stability of the salan complexes (when compared to the salen) due to the presence of amines instead of imines. These results led us to develop other vanadium−salan complexes, to study their structural properties, and to test them in oxidation catalysis. Due to their increased stability and resistance to hydrolysis, the V−salan systems may present advanges over their V−salen counterparts, namely, for the preparation of heterogeneous catalysts by immobilization of the complexes.

In catalytic terms, not much work has been done with salan complexes: Katsuki et al. reported the Ti−salan-catalyzed asymmetric epoxidation of unfunctionalized olefins using aqueous H_2O_2 as a terminal oxidant, with enantioselectivities of up to 98% enantiomeric excess (ee) for several olefins.[16] This group also reported the potential of an Fe(II)−salan−H_2O_2 system in the sulfoxidation of thioanisole, with ee's as high as 96%.[16] Dai et al. reported the catalytic asymmetric addition of organogallium to aldehydes, also with a chiral Ti−salan complex, with moderate to good chemical yields and enantioselectivities (up to 84% ee).[17] Yeori et al. studied the application of Ti−salan complexes in the formation of benzyl ethyl alcohol from benzaldehyde and $Zn(Et)_2$,[18] and the Zr−salan complexes in polymerization reactions.[19]

Sun et al.[20] reported an efficient asymmetric oxidation of sulfides catalyzed by vanadium−salan systems. The catalyst was formed in situ from the reaction of $VO(acac)_2$ (acac = acetylacetonato) and the chiral ligands. The reported enantiomeric excesses (ee %) were good, and the mechanisms proposed involve V^{IV} complexes and binding of the sulfoxide formed to the vanadium center. However, we were unable to reproduce any of these results. Moreover, the preferred enantiomer formed does not agree with that obtained in our experiments, and the recent work of Bryliakov et al.[21] also contests several of the results reported by Sun et al.

Although vanadium−salan complexes have considerable potential as asymmetric catalysts, their characterization has not been reported. In this work, we report the synthesis and characterization of chiral vanadium salen and salan complexes derived from salycylaldehyde and chiral diamines: diaminocyclohexane and diphenylethylenediamine. They present an interesting behavior: in solution, they oxidize to V^V species that we tried to identify by spectroscopic techniques; upon standing, dinuclear species linked by a μ-oxo bridge are formed in the solid state. Catalytic and DFT theoretical studies were carried out and are also reported.

(1) (a) Katsuki, T. *Coord. Chem. Rev.* **1995**, *140*, 189–214. (b) Canali, L.; Sherrington, D. C. *Chem. Soc. Rev.* **1999**, *28*, 85–93.

(2) (a) Cormac, T. D.; Kenneth, M. R.; Valerie, M. W.; Claudine, B.; Declan, G. G. *Top. Catal.* **1998**, *V5*, 75–91. (b) Cozzi, P. G. *Chem. Soc. Rev.* **2004**, *33*, 410–421. (c) Larrow, J. F.; Jacobsen, E. N. *Top. Organomet. Chem.* **2004**, *6*, 123–152.

(3) (a) Cohen, C. T.; Chu, T.; Coates, G. W. *J. Am. Chem. Soc.* **2005**, *27*, 10869–10878. (b) Gröger, H. *Chem. Rev.* **2003**, *103*, 2795–2828. (c) Sammis, G. M.; Jacobsen, E. N. *J. Am. Chem. Soc.* **2003**, *125*, 4442–4443. (d) Sun, W.; Wang, H.; Xia, C.; Li, J.; Zhao, P. *Angew. Chem., Int. Ed.* **2003**, *42*, 1042–1044. (e) Sammis, G. M.; Danjo, H.; Jacobsen, E. N. *J. Am. Chem. Soc.* **2004**, *126*, 9928–9929. (f) Wang, S.-X.; Wang, M.-X.; Wang, D.-X.; Zhu, Z. *Angew. Chem., Int. Ed.* **2008**, *47*, 388–391.

(4) (a) Nakajima, K.; Kojima, M.; Fujita, J. *Chem. Lett.* **1986**, 1483–1486. (b) Nakajima, K.; Kojima, M.; Kojima, K.; Fujita, J. *Bull. Chem. Soc. Jpn.* **1990**, *63*, 2620–2630.

(5) Palucki, M.; Hanson, P.; Jacobsen, E. N. *Tetrahedron Lett.* **1992**, *33*, 7111–7114.

(6) Kokubo, C.; Katsuki, T. *Tetrahedron* **1996**, *52*, 13895–13900.

(7) Correia, I.; Costa Pessoa, J.; Duarte, M. T.; Henriques, R. T.; Piedade, M. F. M.; Veiros, L. F.; Jakusch, T.; Kiss, T.; Dornyei, A.; Castro, M. M. C. A.; Geraldes, C. F. G. C.; Avecilla, F. *Chem.−Eur. J.* **2004**, *10*, 2301–2317.

(8) Correia, I.; Costa Pessoa, J.; Duarte, M. T.; Piedade, M. F. M.; Jackush, T.; Kiss, T.; Castro, M. M. C. A.; Geraldes, C. F. G. C.; Avecilla, F. *Eur. J. Inorg. Chem.* **2005**, 732–744.

(9) Atwood, D. A. *Coord. Chem. Rev.* **1997**, *165*, 267–296.

(10) Klement, R.; Stock, F.; Elias, H.; Paulus, H.; Pelikan, P.; Valko, M.; Mazur, M. *Polyhedron* **1999**, *18*, 3617–3628.

(11) Valko, M.; Klement, R.; Pelikan, P.; Boca, R.; Dlhan, L.; Bottcher, A.; Elias, H.; Muller, L. *J. Phys. Chem.* **1995**, *99*, 137–143.

(12) Bottcher, A.; Elias, H.; Jager, E. G.; Langfelderova, H.; Mazur, M.; Muller, L.; Paulus, H.; Pelikan, P.; Rudolph, M.; Valko, M. *Inorg. Chem.* **1993**, *32*, 4131–4138.

(13) Correia, I.; Dornyei, A.; Jakusch, T.; Avecilla, F.; Kiss, T.; Costa Pessoa, J. *Eur. J. Inorg. Chem.* **2006**, 2819–2830.

(14) Bottcher, A.; Elias, H.; Muller, L.; Paulus, H. *Angew. Chem., Int. Ed.* **1992**, *31*, 623–625.

(15) Correia, I.; Dornyei, A.; Avecilla, F.; Kiss, T.; Costa Pessoa, J. *Eur. J. Inorg. Chem.* **2006**, 656–662.

(16) (a) Sawada, Y.; Matsumoto, K.; Kondo, S.; Watanabe, H.; Ozawa, T.; Suzuki, K.; Saito, B.; Katsuki, T. *Angew. Chem.* **2006**, *118*, 3558–3560. (b) Katsuki, T.; Matsumoto, K.; Ohara, Y.; Kondo, S.; Shimada, Y. *Synlett.* **2007**, *15*, 2445–2447.

(17) Dai, Z.; Zhu, C.; Yang, M.; Zheng, Y.; Pan, Y. *Tetrahedron: Asymmetry* **2005**, *16*, 605–608.

(18) Yeori, A.; Groysman, S.; Goldberg, I.; Kol, M. *Inorg. Chem.* **2005**, *44*, 4466–4468.

(19) (a) Yeori, A.; Goldberg, I.; Shuster, M.; Kol, M. *J. Am. Chem. Soc.* **2006**, *128*, 13062–13063. (b) Segal, S.; Yeori, A.; Shuster, M.; Rosenberg, Y.; Kol, M. *Macromolecules* **2008**, *41*, 1612–1617.

(20) Sun, J. T.; Zhu, C. J.; Dai, Z. Y.; Yang, M. H.; Pan, Y.; Hu, H. W. *J. Org. Chem.* **2004**, *69*, 8500–8503.

(21) Bryliakov, K. P.; Talsi, E. P. *Eur. J. Org. Chem.* **2008**, 3369–3376.

Experimental Section

Materials. Almost all chemicals used were obtained from Merck, Sigma-Aldrich, or Rocc and were of reagent grade. They were used without further purification.

The amine enantiomers were separated according to a literature procedure.[22]

Physical and Spectroscopic Studies. IR spectra were recorded with a BioRad FTS 3000 MX FTIR spectrometer. Visible spectra were recorded with either a Hitachi U-2000, a Shimadzu UV-2401PC, or a Perkin-Elmer Lambda 9 spectrophotometer. The circular dichroism (CD) spectra were run on a Jasco 720 spectropolarimeter, either with the 200−700 nm or with the 400−1000 nm photomultipliers. The temperature was controlled at 25 °C using thermostatized sample compartments with either a Julabo F12 or a Grant GD120 LTC1 thermostatic bath circulator. The cells used were of either 1, 2, 5, or 10 mm optical path. For the samples more susceptible to air oxidation, anaerobic cells (with quartz- and pyrex-graded seals and a takeoff) were used. The electron paramagnetic resonance (EPR) spectra were recorded at 77 K (on glasses made by freezing solutions in liquid nitrogen) with a Bruker ESP 300E X-band spectrometer. The ^{1}H NMR and ^{51}V NMR spectra were recorded on a Bruker Avance+ 400 MHz instrument. The identity of the catalytic products in alkene oxidations was confirmed using a gas chromatography mass spectrometry model Perkin-Elmer Clarus 500 and comparing the fragments of each product with the library available. A Thermax Nicolet gas chromatograph with an HP-1 capillary column (30 m × 0.25 mm × 0.25 μm) was used to analyze the reaction products. Each catalytic experiment was repeated two times to validate the data. The analysis of products in sulfoxidations was done using high-performance liquid chromatography (HPLC; Jasco system: two 880-PU Intelligent HPLC Pumps, a two-line degasser 880−51, and an 870-UV Intelligent UV−vis detector), a Rheodyne 725i injector (5 μL), and Borwing software, using a Daicel Chiralpak IA column.

Synthesis of the Salen-Type Compounds. The Schiff base compounds, sal(*R*,*R*-chen) or sal(*S*,*S*-chen) **1a**, sal(*S*,*S*-dpen) **2a**, Etvan(*S*,*S*-chen) **3a**, and mvan(*S*,*S*-chen) **4a** (see Scheme 1), were prepared following a literature procedure[23] by reaction of the appropriate *o*-hydroxyaldehyde with the optically active diamine (2:1) in methanol. The numbering system used is **N** for salan, **Nb** for salan·2Cl$^-$, and **Na** for salen compounds. For compounds where the molecular structures were determined by X-ray diffraction, **Nc** is used. Most compounds were also prepared as hydrochloride salts, and their protonation state or charge is normally not specified unless we need to emphasize it (e.g., H_2salchan^{2+}·2Cl$^-$ is normally represented as salchan). Their synthesis and characterization by ^{1}H NMR is included in the Supporting Information.

Synthesis of the Salen-Type Compounds. sal(*R*,*R*-chan) or sal(*S*,*S*-chan) (1 and 1b). sal(*R*,*R*-chen) or sal(*S*,*S*-chen) (**1a**) was dissolved in MeOH, and a slight excess of $NaBH_4$ was slowly added. The reduction was considered complete when the solution became colorless. The pH was then adjusted to 1−1.5 with an aqueous 4 M HCl solution. The solvent was evaporated and the white residue extracted with an ethanol/diethyl ether (70:30) liquid phase, the inorganic solids being separated by filtration. By evaporation of the solvent, a white solid was obtained. Yield: 78%. ^{1}H NMR-D_2O: 1.43, 1.73, 2.25, 2.29 [8H, s, $-CH_2-$], 3.57 [2H, s, $CH_2CH-N^+H_2$], 4.11, 4.15 [2H, d, J_{HH} = 16 Hz, Ar−CH_AH−N^+H_2], 4.26, 4.29 [2H, d, J_{HH} = 12 Hz, Ar−CH_BH−N^+H_2], 6.95 [4H, m, aromatic], 7.33 [4H, m, aromatic]. ^{13}C NMR-D_2O: 20.27, 24.39 [4C, $-CH_2-$], 43.76 [2C, Ar−CH_2−NH_2^+], 56.33 [2C, $-(CH_2)_2-CH-NH_2^+$], 114.48, 115.37, 119.63, 130.56, 130.71, 153.85 [12C, aromatic].

H_2sal(*R*,*R*-chan)$^{2+}$·2Cl$^-$·$(CH_3)_2$CHOH·H_2O (1c). Compound **1** was dissolved in isopropanol, and after three weeks, colorless crystals suitable for single-crystal X-ray diffraction were separated and washed with diethyl ether.

sal(*S*,*S*-dpan) (2 and 2b). The compound was obtained as a white solid, similarly to **1**, and it was also converted to the HCl salt. Yield: 78%. ^{1}H NMR-DMSO-d_6 for sal(*S*,*S*-dpan): 3.59 [2H, t, J_{HH} = 6.6 Hz, Ar−C*H*−NH], 3.68, 3.71 [2H, d, J_{HH} = 12.5 Hz, Ar−CHH_A−NH], 3.87, 3.90 [2H, d, J_{HH} = 12.6 Hz, Ar−CHH_b−NH], 6.77, 6.79, 6.81 [2H, t, J_{HH} = 7.5 Hz, aromatic], 6.88, 6.90 [2H, d, J_{HH} = 7.4 Hz, aromatic], 7.17, 7.18 [2H, d, J_{HH} = 7.4 Hz, aromatic], 7.23 [4H, t, J_{HH} = 2.7 Hz, aromatic], 7.32, 7.33 [2H, d, J_{HH} = 7.3 Hz, aromatic]. ^{13}C NMR-DMSO-d_6: 20.27, 24.39 [4C, $-CH_2-$], 43.76 [2C, Ar−CH_2−NH_2^+], 56.33 [2C, $-(CH_2)_2-CH-NH_2^+$], 114.48, 115.37, 119.63, 130.56, 130.71, 153.85 [12C, aromatic].

Etvan(*S*,*S*-chen) (3c). A small amount of **3a** was dissolved in acetonitrile. After ca. 4 weeks, the crystals that formed were separated, washed with small amounts of water, and used for the single-crystal X-ray diffraction study.

Etvan(*S*,*S*-chan)$^{2+}$·2Cl$^-$ (3 and 3b). This was obtained similarly to **1**. A light-brown solid was obtained. Yield: 64%. ^{1}H NMR-DMSO-d_6: 1.37 [6H, t, J_{HH} = 6.6 Hz, $-CH_3$], 1.38, 1.63, 1.83, 2.02 [8H, s, $-CH_2-$], 3.58 [2H, s, $-CH_2CH-N^+$], 4.10 [4H, q, J_{HH} = 6.8 Hz, $-CH_2-O$] [8H, s, $-CH_2-$], 4.12, 4.15, [2H, d, J_{HH} = 12.6 Hz, Ar−CH_aH−N^+H_2], 4.29, 4.32 [2H, d, J_{HH} = 12.6 Hz, Ar−CH_aH−N^+H_2], 6.95 [2H, m, aromatic], 7.08 [2H, d, J_{HH} = 7.5 Hz aromatic]. ^{13}C NMR-DMSO-d_6: 15.40, 15.49 [2C,

Scheme 1. Molecular Formulas of Some of the Salen- and Salan-Type Compounds Prepared[a]

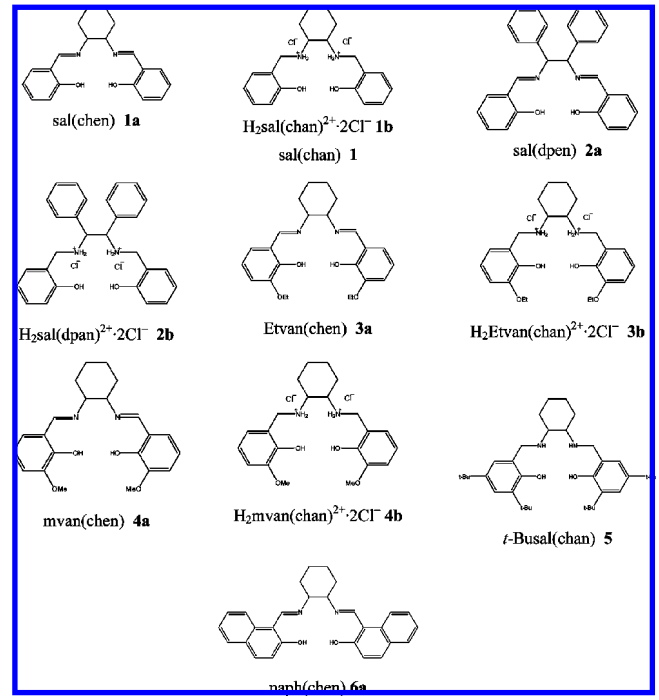

[a] The protonation state of the compounds is omitted except when this is relevant for the discussion. The numbering system used is **N** for salan, **Nb** for salan·2Cl$^-$, and **Na** for salen compounds.

(22) Poddar, S. N.; Day, K.; Sarkar, S. C. N. *J. Indian Chem. Soc.* **1963**, *40*, 489.
(23) Galsbøl, F.; Steenbøl, P.; Sørensen, B. S. *Acta Chem. Scand.* **1972**, *26*, 3605–3611.

Table 1. Oxovanadium(IV) Complexes Prepared, Yields, Colors, Formulations, and Elemental Analysis [calculated values for the specified formula between parentheses]

compound	η (%)	color	%C, %H, %N	formula
$V^{IV}O${sal(chen)} **7a**	64	turkish-blue	60.5 (60.6), 5.7 (5.3), 6.9 (7.1)	$C_{20}H_{20}N_2O_3V\cdot0.5H_2O$
$V^{IV}O${sal(dpen)} **8a**	50	brown	68.9 (68.8), 5.1 (4.6), 5.9 (5.7)	$C_{28}H_{22}N_2O_3V\cdot H_2O$
$V^{IV}O${sal(chan)} **7**	79	brown	59.0 (58.7), 6.6 (6.4), 6.8 (6.8)	$C_{20}H_{24}N_2O_3V\cdot1H_2O$
$V^{IV}O${sal(dpan)} **8**	80	brown	57.3 (57.8), 5.0 (4.9), 4.8 (4.8)	$C_{28}H_{26}N_2O_3V\cdot1H_2O$
$V^{IV}O${Etvan(chen)} **9a**	64	green	54.9 (55.0), 5.8 (5.8), 5.4 (5.2)	$C_{24}H_{28}N_2O_5V\cdot1H_2O\cdot0.5CH_2Cl_2$
$V^{IV}O${Etvan(chan)} **9**	70	brown	58.1 (58.0), 6.9 (6.9), 5.4 (5.6)	$C_{24}H_{32}N_2O_5V\cdot1H_2O$
$V^{IV}O${mvan(chen)} **10a**	95	green	56.0 (56.0), 6.4 (6.5), 5.8 (5.8)	$C_{22}H_{24}N_2O_5V\cdot2.5MeOH$
$V^{IV}O${mvan(chan)} **10**	90	brown	56.1 (56.1), 6.9 (6.8), 5.8 (5.7)	$C_{22}H_{28}N_2O_5V\cdot0.5H_2O\cdot$ 1MeOH
$V^{IV}O${naph(chan)} **11**	80	grey	61.6 (61.6), 6.3 (6.6), 4.1 (4.7)	$C_{28}H_{28}N_2O_3V\cdot1.4H_2O\cdot$ 2.3MeOH
$V^{IV}O${*t*Busal(chan)} **12**	70	grey	71.4 (71.6), 10.3 (10.0), 3.9 (4.0)	$C_{36}H_{56}N_2O_3V\cdot1C_5H_{12}$
{$V^{V}O$[sal(chan)]}$_2(\mu$-O)} **13**	67	dark-red	58.8 (58.8), 6.6 (6.2), 6.7 (6.9)	$C_{40}H_{48}N_4O_7V_2\cdot1H_2O$

CH_3CH_2O-], 23.27, 27.10 [4C, $-CH_2-$], 44.80 [2C, Ar$-CH_2-NH_2^+$], 57.81 [2C, $-(CH_2)_2-CH-NH_2^+$], 65.61 [2C, CH_3CH_2O-], 115.37, 118.60, 121.35, 123.85, 145.84, 147.68 [12C, aromatic].

mvan(*S*,*S*-chan)$^{2+}\cdot2Cl^-$ (4 and 4b). This was obtained similarly to **1**. A light-brown solid was obtained. Yield: 65%. ^{1}H NMR-D_2O: 1.47, 1.76, 2.25, 2.28 [8H, s, $-CH_2-$], 3.58 [2H, t, J_{HH} = 3.2 Hz, $-CH_2CH-N^+$], 3.85 [6H, s, CH_3O-], 4.19, 4.23, [2H, d, J_{HH} = 13.2 Hz, Ar$-CH_aH-N^+H_2$], 4.33, 4.37 [2H, d, J_{HH} = 13.2 Hz, Ar$-CHH_b-N^+H_2$] 6.91 [4H, m, aromatic], 7.1 [2H, dd, J_{1HH} = 7.7 Hz, J_{2HH} = 1.8 Hz aromatic]. ^{13}C NMR-D_2O: 20.27, 24.39 [4C, $-CH_2-$], 43.76 [2C, Ar$-CH_2-NH_2^+$], 54.57 [2C, CH_3O-], 55.33 [2C, $-(CH_2)_2-CH-NH_2^+$], 112.68, 115.37, 119.59, 121.85, 143.28, 146.29 [12C, aromatic].

***t*-Busal(*R*,*R*-chan) (5 and 5b).** The tartrate of 1*R*,2*R*-diaminocyclohexane was dissolved in MeOH, and 2 equiv of aqueous $NaHCO_3$ was added. In a separate flask, 2 equiv of 2,4-di-*t*-butylphenol was dissolved in MeOH, and 4 equiv of formaldehyde (37% methanolic solution) were added. The two solutions were mixed and refluxed for 3 h. A viscous mixture formed, which was washed with water and small amounts of MeOH and diethyl ether. A solid was obtained to which HCl in ethanol was added, and the mixture was heated for ca.1 h. The mixture was cooled down, and after the addition of diethyl ether, a white precipitate was obtained. Yield: 91%. ^{1}H NMR-DMSO-d_6: 1.19, 1.23, 1.30, 1.33 [36H, s, Ar$-C(CH_3)_3$], 1.79, 2.36 [8H, s, $-CH_2-$], 3.69 [2H, s, CH_2CH-N^+H2] 4.18, [2H, s, Ar$-CH_2-N^+H_2$], 4.28, [2H, s, Ar$-CH_2-N^+H_2$], 7.22, 7.46 [4H, s, aromatic]. ^{13}C NMR-DMSO-d_6 (HCl salt): 22.05, 25.51 [4C, $-CH_2-$], 29.88, 31.33 [12C, Ar$-C(CH_3)_3$], 34.07, 34.75 [4C, Ar$-C(CH_3)_3$], 44.35, [2C, Ar$-CH_2-NH_2^+$], 56.49 [2C, $-(CH_2)_2-CH-NH_2^+$], 121.56, 124.10, 127.11, 139.22, 142.33, 151.60 [12C, aromatic].

naph(*R*,*R*-chen) (6c). The compound naph(*R*,*R*-chen) was dissolved in a small amount of methanol and left to evaporate in the air at room temperature. After ca. 3 weeks, the yellow crystals obtained were filtered, washed with small amounts of water, and used for single-crystal X-ray diffraction studies.

The elemental analyses for the compounds mentioned above are presented in the Supporting Information.

Synthesis of the Oxovanadium(IV) Complexes. All preparations with oxovanadium(IV) were carried out under nitrogen. The general procedure for the synthesis of oxovanadium(IV) complexes **7**−**12** (see Table 1) is as follows: the ligand (1 equiv) was dissolved in MeOH. Then, 1.1 equiv of $VOCl_2$ (50% aqueous solution) was added, and the pH was adjusted using 1 M NaOH. The desired oxovanadium(IV) complex then precipitated. The complex was filtered, washed with methanol and water, and dried under vacuum. Table 1 lists the compounds prepared, their yields, colors, elemental analyses, and formulations.

Synthesis of the Oxovanadium(V) Complexes. [{$V^{V}O$[sal(*R*,*R*-chan)]}$_2(\mu$-O)]$\cdot1H_2O$ (13). A total of 0.5 g of **7** was dissolved in 20 mL of CH_2Cl_2 with vigorous stirring under air. After 24 h, the solution was dark red-brown. The solvent was then evaporated to dryness and the residue washed with water, small amounts of MeOH, and *n*-hexane and dried under vacuum. Yield ca. 25%. ESI-MS+: *m*/*z* 391.1 [VOL$^+$, 100%].

[{$V^{V}O$[sal(*S*,*S*-dpan)]}$_2(\mu$-O)]$\cdot H_2O\cdot2(CH_3)_2CHOH$ (14c). The $V^{IV}O$ complex **8** was dissolved in a 7:3 mixture of CH_2Cl_2/isopropanol and was left in the air. After slow and partial evaporation of the solvent, which took ca. 3 weeks, the black needles obtained were filtered, washed with small amounts of water, and used for single-crystal X-ray diffraction studies. ESI-MS+: *m*/*z* 425.2 [LH$^+$, 100%], 489.0 [VOL$^+$, 25%], 998.3 [(VOL)$_2$O − 4H$^+$].

[{$V^{V}O$[*t*-Busal(*R*,*R*-chan)]}$_2(\mu$-O)]$\cdot2(CH_3)_2CHOH$ (15c). Black crystals were obtained similarly to **14c** from the $V^{IV}O$ complex **12**. ESI-MS+ *m*/*z* 551.5 [LH$^+$, 60%], 615.5 [VOL$^+$, 100%]. ESI-MS−: *m*/*z* 548.5 [L$^-$, 100%], 1244.5 [$V_2O_3L_2^{2-}$, 50%].

EPR Spectroscopy. The $V^{IV}O$ EPR spectra were simulated using a program from Rockenbauer and Korecz.[24] The EPR spectra help to elucidate which groups coordinate in solution.[25,26] For the $V^{IV}O$ systems, we used the additivity rule to estimate the hyperfine coupling constant $A_{\parallel}^{est}$, based on the contributions $A_{\parallel,i}$ of each of the four equatorial donor groups [$A_{\parallel}^{est} = \sum A_{\parallel,i}$ (i = 1−4)]. The estimated accuracy of $A_{\parallel}^{est}$ is 3×10^{-4} cm^{-1}.[25] These data can be used to establish the most probable binding mode of the V^{IV} complexes in solution.

^{1}H and ^{51}V NMR Spectroscopy. The NMR samples were prepared at room temperature immediately before NMR spectroscopic measurements, except those where the oxidation of the V^{IV} to V^{V} species was being studied. The solutions containing the V^{V} complexes were prepared weighting the adequate amount of the complex and dissolving it in the selected solvent to obtain ^{51}V NMR spectra. The ^{1}H and ^{51}V NMR chemical shifts were referenced relative to TSS (sodium 3-(trimethylsilyl)propane sulfonate) and to a neat $VOCl_3$ external reference at 0 ppm, respectively.

X-Ray Crystal Structure Determination. Three-dimensional X-ray data for **1c**, **3c**, and **14c** were collected on a Bruker Smart 1000 CCD diffractometer using the ω scan method and **6c** and **15c** on a Bruker Kappa X8Apex CCD diffractometer using the $\phi-\omega$ scan method. Data were collected at room temperature. Reflections were measured from a hemisphere of data collected of frames, each covering 0.3° in ω. Of the 9352 in **1c**, 14 827 in **3c**, 21 766 in **6c**,

(24) Rockenbauer, A.; Korecz, L. *Appl. Magn. Reson.* **1996**, *10*, 29–43.
(25) Chasteen, N. D. *Biological Magnetic Resonance*; Lawrence, J., Berliner L. J., Reuben, J., Eds.; Plenum: New York, 1981; Chapter 2, pp 53−119.
(26) (a) Smith, T. S.; Root, C. A.; Kampf, J. W.; Rasmussen, P. G.; Pecoraro, V. L. *J. Am. Chem. Soc.* **2000**, *122*, 767–775. (b) Rehder, D. *Bioinorganic Vanadium Chemistry*; John Wiley & Sons: Chicheter, U. K., 2008.

Table 2. Crystal and Structure Refinement Data[a] of Compounds **1c**, **3c**, **6c**, **14c**, and **15c** with Structure Determined by Single-Crystal X-Ray Diffraction

	H_2sal(chan)$^{2+}\cdot 2Cl^-$, **1c**	Etvan(chen), **3c**	naph(chen), **6c**	$\{V^VO[sal(dpan)]\}_2(\mu\text{-O})$, **14c**	$\{V^VO[t\text{-Busal(chan)}]\}_2(\mu\text{-O})$, **15c**
formula	$C_{23}H_{38}Cl_2N_2O_4$	$C_{24}H_{30}N_2O_4$	$C_{28}H_{26}N_2O_2$	$C_{61.25}H_{66}N_4O_{9.75}V_2$	$C_{78}H_{126}N_6O_9V_2$
M_r	477.45	410.50	422.51	1116.06	1393.73
T [K]	100(2)	100(2)	100(2)	100(2)	100(2)
λ, Å [Mo, K_α]	0.71073	0.71073	0.71073	0.71073	0.71073
cryst syst	monoclinic	triclinic	orthorhombic	monoclinic	monoclinic
space group	$P2_1$	$P\bar{1}$	$P2_12_12_1$	$C2$	$P2_1/c$
a [Å]	9.0813(4)	10.0324(4)	9.3699(7)	24.8548(19)	19.503(5)
b [Å]	16.0307(7)	11.5043(5)	9.4651(8)	13.8673(11)	16.308(5)
c [Å]	9.8496(4)	11.7327(5)	25.339(2)	33.590(3)	25.577(5)
α [deg]	90	116.1610(10)	90	90	90
β [deg]	117.3800(10)	109.6540(10)	90	98.3800(10)	103.283(5)
γ [deg]	90	97.3130(10)	90	90	90
Z	2	2	4	2	4
volume [Å^3]	1273.27(9)	1082.07(8)	2247.2(3)	11453.9(15)	7917(4)
ρ_{calcd}[gcm^{-3}]	1.245	1.245	1.260	1.294	1.169
μ mm^{-1}	0.285	0.086	0.079	0.387	0.292
reflns measured	9352	14827	21766	64390	57358
independent refls[b]	4232	4118	2679	19287	9999
R(int)	0.0149	0.0297	0.0448	0.0651	0.0739
goodness of fit on F^2	1.033	1.043	1.116	1.035	1.160
R_1[c]	0.0341	0.0397	0.0362	0.0670	0.0703
wR_2 (all data)[c]	0.0920	0.1020	0.1108	0.1852	0.2174

[a] All structures were solved using SHELXS program for crystal structure determination[27] and refined with SHELXL program for crystal structure refinement.[29] [b] $I > 2\sigma(I)$. [c] $R_1 = \sum ||F_o| - |F_c||/\sum|F_o|$, $wR_2 = \{\sum[w(|F_o|^2 - |F_c|^2)^2]/\sum[w(F_o^4)]\}^{1/2}$.

64 390 in **14c**, and 57 358 in **15c** reflections measured, all of which were corrected for Lorentz and polarization effects, and for absorption by semiempirical methods based on symmetry-equivalent and repeated reflections, 4232 in **1c**, 4118 in **3c**, 2679 in **6c**, 19 287 in **14c**, and 9999 in **15c** independent reflections exceeded the significance level $|F|/\sigma(|F|) > 4.0$. Complex scattering factors were taken from the program package SHELXTL.[27] For **1c**, **14c**, and **15c** the absolute configuration was established by refinement of the enantiomorph polarity parameter [$x = -0.01(5)$ for **1c**, 0.031(17) for **14c**, and 0.000(10) for **15c**].[28] The structures were solved by direct methods and refined by full-matrix least-squares methods on F^2. The non-hydrogen atoms were refined with anisotropic thermal parameters in all cases, except for C10S, C11S, C12S, O4S, O1W, and O2W solvent molecules in **14c**. The hydrogen atoms were included in calculated positions and refined by using a riding mode for C1S, C2S, and C11 and left to refine freely in the other cases in **1c**, and in all cases in **3c** and **6c**. The hydrogen atoms were refined to carbon, oxygen, and nitrogen atoms in **14c** and **15c**, which were placed in idealized positions and refined by using a riding mode, except for C4D, C5D, C8, C13, C14, C49, and C50 in **15c**, which were left to refine freely. A final difference Fourier map showed no residual density outside: +1.277 and −0.583 e·Å^{-3} in **1c**, +0.352 and −0.216 e·Å^{-3} in **3c**, +0.278 and −0.217 e·Å^{-3} in **6c**, +1.244 and −0.620 e·Å^{-3} in **14c**, and +1.003 and −0.784 e·Å^{-3} in **15c**. The crystal of **14c** presents a slight disorder on a $(CH_3)_2CHOH$ solvent molecule. This disorder has been observed and refined with anisotropic atomic displacement parameters in each case. The site occupancy factors were 0.44286 for C1SA and 0.55714 for C1SB. Crystal data and details on data collection and refinement are summarized in Table 2. CCDC 693398 (for **1c**), 693399 (for **3c**), 693401 (for **6c**), 693400 (for **14c**), and 693402 (for **15c**) contain the supplementary crystallographic data for this paper, as does section SI-2 of the Supporting Information. These data can be obtained free of charge from the Cambridge Crystallographic Data Centre via www.ccdc.cam.ac.uk/data_request/cif.

DFT Computational Details. The full geometry optimization of V−salan model complexes and transition states has been carried out at the DFT level of theory using Becke's three-parameter hybrid exchange functional[30] in combination with the gradient-corrected correlation functional of Lee, Yang, and Parr[31] (B3LYP) with the help of the Gaussian 98[32] program package. Symmetry operations were not applied for all structures. The geometry optimization was carried out using a relativistic Stuttgart pseudopotential describing 10 core electrons and the appropriate contracted basis set (8s7p6d1f)/[6s5p3d1f][33] for the vanadium atom and the 6-31G(d) basis set for other atoms. Then, single-point calculations were performed with the 6-311+G(d,p) basis set on the nonmetal atoms, and solvent effects were taken into account by using the polarizable continuum model[34] in the CPCM version[35] with CH_3CN as a solvent. The Hessian matrix was calculated analytically for all optimized structures in order to prove the location of the correct minimum (no "imaginary" frequencies) or saddle points (only one negative eigenvalue).

(27) Sheldrick, G. M. *SHELXS-97*, revision 5.1; University of Göttingen: Göttingen, Germany, 1997.

(28) (a) Flack, H. D.; Bernardinelli, G. *Acta Crystallogr., A* **1999**, *A55*, 908–915. (b) Flack, H. D.; Bernardinelli, G. *J. Appl. Crystallogr.* **2000**, *33*, 1143–1148.

(29) Sheldrick, G. M. *SHELXL-97*, revision 5.1; University of Göttingen: Göttingen, Germany, 1997.

(30) Becke, A. D. *J. Chem. Phys.* **1993**, *98*, 5648–5652.

(31) Lee, C.; Yang, W.; Parr, R. G. *Phys. Rev. B: Condens. Matter Mater. Phys.* **1988**, *37*, 785–789.

(32) Frisch, M. J.; Trucks, G. W.; Schlegel, H. B.; Scuseria, G. E.; Robb, M. A.; Cheeseman, J. R.; Zakrzewski, V. G.; Montgomery, J. A., Jr.; Stratmann, R. E.; Burant, J. C.; Dapprich, S.; Millam, J. M.; Daniels, A. D.; Kudin, K. N.; Strain, M. C.; Farkas, O.; Tomasi, J.; Barone, V.; Cossi, M.; Cammi, R.; Mennucci, B.; Pomelli, C.; Adamo, C.; Clifford, S.; Ochterski, J.; Peterson, G. A.; Ayala, P. Y.; Cui, Q.; Morokuma, K.; Malick, D. K.; Rabuck, A. D.; Raghavachari, K.; Foresman, J. B.; Cioslowski, J.; Ortiz, J. V.; Baboul, A. G.; Stefanov, B. B.; Liu, G.; Liashenko, A.; Piskorz, P.; Komaromi, I.; Gomperts, R.; Martin, R. L.; Fox, D. J.; Keith, T.; Al-Laham, M. A.; Peng, C. Y.; Nanayakkara, A.; Challacombe, M.; Gill, P. M. W.; Johnson, B.; Chen, W.; Wong, M. W.; Andres, J. L.; Gonzalez, C.; Head-Gordon, M.; Replogle, E. S.; Pople, J. A. *Gaussian 98*, revision A.9; Gaussian Inc.: Pittsburgh, PA, 1998.

(33) Dolg, M.; Wedig, U.; Stoll, H.; Preuss, H. *J. Chem. Phys.* **1987**, *86*, 866–872.

(34) Tomasi, J.; Persico, M. *Chem. Rev.* **1994**, *94*, 2027–2094.

(35) Barone, V.; Cossi, M. *J. Phys. Chem. A* **1998**, *102*, 1995–2001.

Catalytic Activity Studies. All catalytic reactions for the oxidation of styrene, cyclohexene, and cumene were carried out using 50 mL double-neck reaction flasks fitted with a septum and a water condenser. In a typical reaction (see Results and Discussion section), styrene (0.52 g, 5 mmol), aqueous 30% H_2O_2 (1.13 g, 10 mmol), and the catalyst (0.10 mmol) were mixed in CH_3CN (10 mL), and the reaction was carried out at 80 °C, with stirring. During the course of the reaction, 0.5 mL of the reaction mixture were withdrawn every half hour, extracted with petroleum ether (5 × 2 mL), and analyzed quantitatively by gas chromatography.

The catalytic reactions for oxidation of thioanisole were carried out in a thermostatized STEM Omni-Reacto Station (OS1025) using 25 mL reaction vessels. Normally (see the Results and Discussion section), 0.0025 to 0.1 mmol of the catalyst and 4 mL of the solvent were introduced, and 1 mmol of thioanisole was dissolved. Then, 1.2−1.5 mmol of an aqueous solution of H_2O_2 (20% w/v, ca. 230 μL) was added (time = 0). The reactions were carried out with vigorous stirring, in the presence of air, at the selected temperature over 24 h. In some cases, the H_2O_2 solution was added in portions of 10 μL every 20 min. The progress of the sulfoxidations was followed using chiral HPLC with a Daicel Chiralpak IA column, with the eluent hexane/ethyl acetate (60:40), at a flow rate of 1 mL/min. The calibration curves for each reagent and product, namely, the sulfide, sulfoxide, and sulfone, were determined using similar HPLC procedures, and these calibrations were used for the quantitative analyses. Diphenylsulfone was used as an internal standard.

Results and Discussion

Ligand Synthesis and Characterization. The synthesis of the salen-type compounds involved the reaction of the aromatic aldehyde with the diamine, either 1*R*,2*R*-diaminocyclohexane, 1*S*,2*S*-diaminocyclohexane, or 1*S*,2*S*-diphenylethylenediamine. Their formulas and abbreviations are shown in Scheme 1. The synthesis of the salan ligands involved either the reduction of the salen parent compounds with $NaBH_4$ and their conversion to the HCl salts or a Mannich-type condensation[36] between formaldehyde, the diamine, and a substituted phenol (e.g., ligand **5**). They were prepared in good to high yields, gave satisfactory elemental analysis, and were characterized by spectroscopic techniques: ^{1}H NMR, FTIR, UV, and CD.

In the ^{1}H NMR spectra, the peaks attributed to the CH_2−N groups of salan-type compounds appear at ∼4 ppm, and the CH═N peaks were not detected, confirming the reduction of the imine bond. The FTIR spectra also do not show the ν(C═N) band, and the ν(N−H) appears at ca. 3220 cm^{-1}, or under a broad band centered at ca. 3400 cm^{-1} (this due to the H_2O and phenolic OH groups).

In the electronic absorption spectra (see Table SI-1-2, Supporting Information), the C═N bond, which in the spectra of the parent salen ligands is responsible for the $n \rightarrow \pi^*$ and $\pi \rightarrow \pi^*$ transitions (at ca. 400 and 320 nm for the salicylaldehyde derivatives, respectively), is not detected. In the literature, there are almost no data on isotropic UV and CD spectra of salicylaldamines. The salan ligands **1** {sal(*S*,*S*-chan)} and **2** {sal(*S*,*S*-dpan)} show only $\pi \rightarrow \pi^*$ transitions below 300 nm associated with the aromatic rings (see SI-1, Supporting Information). The UV transitions observed are red-shifted when compared to their salen counterparts. In the CD spectra, the rotational strengths of the bands of the salan compounds are much lower than those of their parent salen compounds. In the salen compounds, the extended resonance throughout the imine bonds allows a relatively efficient transmission of chirality to the chromophores, and the CD signals are much more intense. Moreover, the higher flexibility of the salan compounds when compared to the salen also allows the presence of other conformers in equilibrium.

Crystal Structures of Ligands. The single-crystal X-ray structures of two Schiff base compounds, Etvan(*S,S*-chen) (**3c**) and naph(*R*,*R*-chen) (**6c**), and of one reduced Schiff base compound, H_2sal(*R*,*R*-chan)$^{2+}\cdot H_2O\cdot(CH_3)_2CHOH\cdot 2Cl^-$ (**1c**), were determined by single-crystal X-ray diffraction. ORTEP representations are presented in Figure 1, and selected bond lengths and angles are given in Table 3. The molecular structure of the Schiff base compounds Etvan(*S*,*S*-chen) (**3c**) and naph(*R*,*R*-chen) (**6c**) are partly determined by the conjugation between the aromatic rings and the imine bonds of the molecules, which induces planarity in the ligand's "arms". In **1c**, since there is no imine bond, the H_2sal(*R*,*R*-chan)$^{2+}$ molecule is thus much more flexible and distorted.

Crystal Structure of H_2sal(*R*,*R*-chan)$^{2+}\cdot H_2O\cdot(CH_3)_2$-CHOH·2Cl$^-$ (1c). Figure 1 shows a representation of H_2sal(*R*,*R*-chan)$^{2+}$. The molecule is dicationic with two protons in each amine group, and two chloride atoms as counterions. One molecule of water and one isopropanol are also present in the asymmetric unit. The NH_2−CH_2 and O−CH_2 bond lengths of **1c** (Table 3) are consistent with the single-bond N−C and O−C nature of these bonds, and the torsion angles C5−C6−C7−N1 and N2−C14−C15−C16 are −82.49(25)° and −106.85(25)°, respectively. The cyclohexane ring is in the chair conformation with both carbon atoms with an *R*-configuration.

The molecular structure of the compound is partly determined by the intermolecular interactions involving hydrogen bonds (H-bonds) with Cl^- ions and solvent molecules, namely, O−H···Cl and N−H···Cl H-bonds. The intermolecular contacts (H···A) may be categorized as short (H···Cl^- distance, $d \leq 2.52$ Å), intermediate (2.52−2.95 Å), and long (2.95−3.15 Å).[37] In section SI-2 (Supporting Information), we summarize the distances and angles for the H-bonds present in **1c**. These interactions are short in all O−H···Cl and N−H···Cl interactions present in **1c**.

Crystal Structure of Etvan(*S*,*S*-chen) (3c). Figure 1 shows an ORTEP representation of Etvan(*S*,*S*-chen). The asymmetric unit contains one neutral molecule. The N−CH and O−CH_2 lengths of **3c** are consistent with the double-bond nature of N═C and with the single-bond nature of O−C, and the torsion angles C5−C6−C7−N1 and N2−C14−C15−C16 are close to 180°: 174.37(11)° and 173.30(11)°, respectively. In this molecule, the rigid structure of the pendant arms and its planarity (planes defined for N2−C14−

(36) Tshuva, E. Y.; Gendeziuk, N.; Kol, M. *Tetrahedron Lett.* **2001**, *42*, 6405–6407.

(37) Aullón, G.; Bellamy, D.; Brammer, L.; Bruton, E. A.; Orpen, G. *J. Chem. Soc., Chem. Commun.* **1998**, 653–654.

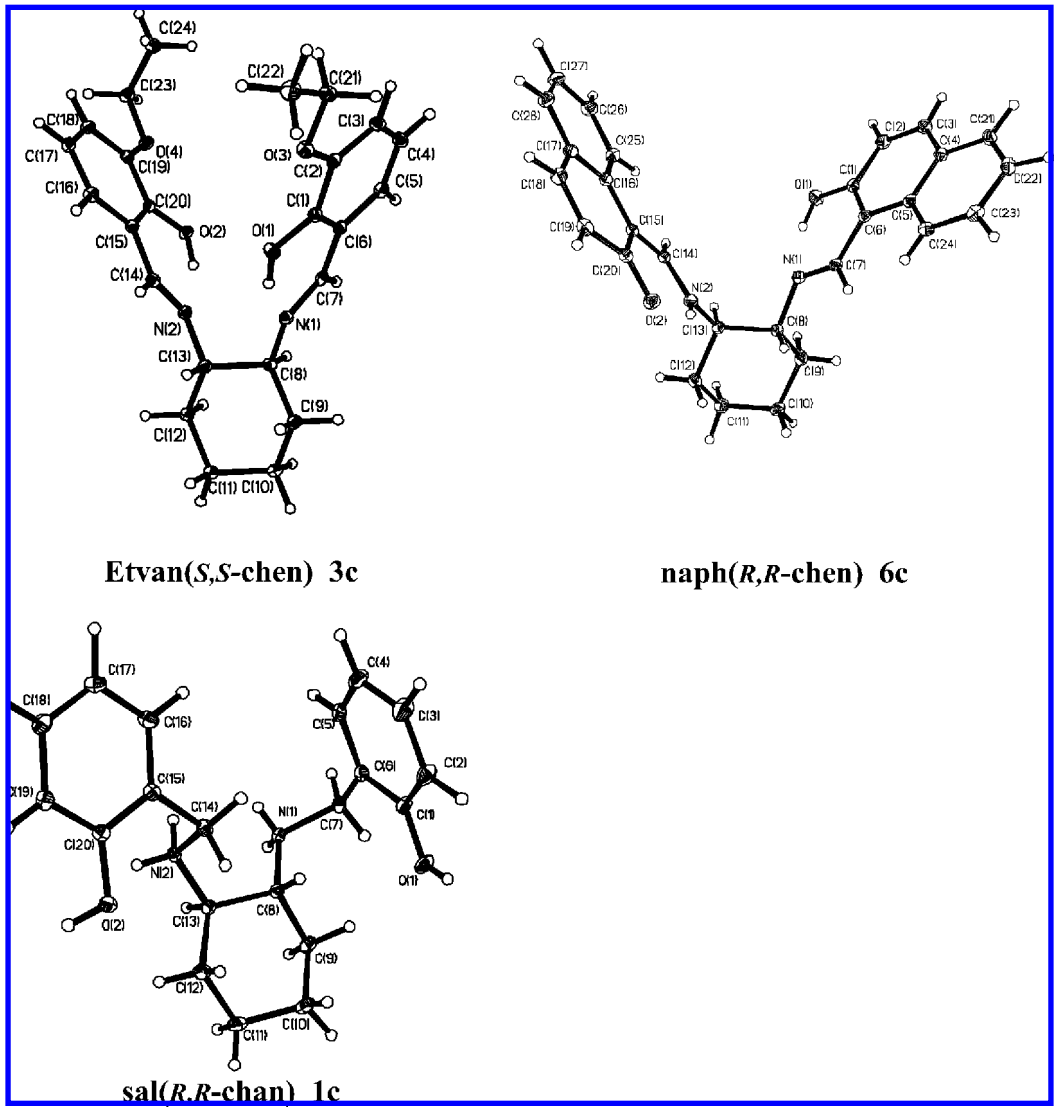

Figure 1. ORTEP diagrams of Etvan(*S*,*S*-chen) **3c**, naph(*R*,*R*-chen) **6c**, and the cation of **1c** H_2sal(*R*,*R*-chan)$^{2+}$ with the thermal ellipsoids of the non-hydrogen atoms drawn at the 30% probability level. In **1c**, the solvent molecules and Cl^- atoms were omitted for clarity.

C15−C20−O2 atoms, mean deviation from plane = 0.0272 Å, and for N1−C7−C6−C1-O1, mean deviation from plane = 0.0258 Å) are determined by the conjugation of the aromatic system with the N=C double bonds and the presence of intramolecular H-bonds between N_{imine} and O_{phenol} atoms. The data for **3c** are summarized in Table 3 and in section SI-2 (Supporting Information).

Crystal Structure of naph(*R*,*R*-chen) (6c). Figure 1 shows a representation of naph(*R*,*R*-chen). The asymmetric unit contains one neutral molecule of naph(*R*,*R*-chen). The N−CH and O−CH_2 lengths of **6c** are consistent with the double-bond nature of N=C and with the single-bond nature of O−C, comparable with the values found for other salen compounds, namely for **3c**. The torsion angles C5−C6−C7−N1 and N2−C14−C15−C16 are also close to 180°: −179.18(22)° and +176.67(20)°, respectively. It is interesting that the imine atom N(2) is bonded to a hydrogen atom, while with N(1) this corresponds to a H-bond [N(1)···H−O]; this explains why the N1−C7 bond is significantly shorter than N2−C14. This structure only presents intramolecular hydrogen bonds between N_{imine} and O_{phenol} atoms, which further determines the rigid structure of the pendant arms and their planarity (planes defined for N2−C14−C15−C20−O2 atoms, mean deviation from plane = 0.0109 Å, and for N1−C7−C6−C1−O1, mean deviation from plane = 0.0133 Å). The data for **6c** is summarized in Table 3 and in section SI-2 (Supporting Information).

Synthesis and Characterization of the Vanadium Complexes. The reaction of the ligands with $VOCl_2$ leads to the formation of $V^{IV}O$ complexes with a N_2O_2 binding mode, in moderate yields. The complexes were characterized by elemental analysis and spectroscopic techniques (see Tables 1 and 4 and Table SI-1, Supporting Information). Compound **13** was obtained by aerobic oxidation of a CH_2Cl_2 solution of the parent $V^{IV}O$ complex **7**. Its elemental analysis fits to a dinuclear formula that is probably similar to those of **14c** and **15c**, which were characterized by single-crystal X-ray diffraction.

Infrared Spectra. All $V^{IV}O$−salen complexes present ν(V=O) at ca. 980 cm^{-1} (see Table 4), and excluding complex **11**, all $V^{IV}O$−salan complexes present the ν(V=O) at ca. 840−890 cm^{-1}. These low ν(V=O) values indicate

Table 3. Selected Bond Lengths (Å) and Angles (deg) for **1c**, **3c**, **6c**, **14c**, and **15c**

H_2sal(chan)$^{2+}$·2Cl$^-$ **1c**		Etvan(chen), **3c**	naph(chen), **6c**	{V^{V}O[sal(chan)]}$_2$(μ-O), **14c**		{V^{V}O[*t*-Busal(chan)]}$_2$(μ-O), **15c**	
				Bond Lengths			
O(1)−C(1)	1.366(3)	1.3533(14)	1.337(3)	O(1)−C(1)	1.370(6)	O(1)−C(1)	1.349(5)
O(2)−C(20)	1.373(3)	1.3529(14)	1.276(3)	O(2)−C(28)	1.347(6)	O(2)−C(20)	1.352(5)
N(1)−C(7)	1.508(3)	1.2793(16)	1.288(3)	O(4)−C(29)	1.364(5)	O(4)−C(56)	1.347(6)
N(1)−C(8)	1.513(3)	1.4617(15)	1.466(3)	O(5)−C(56)	1.357(5)	O(5)−C(37)	1.348(5)
N(2)−C(14)	1.508(3)	1.2749(15)	1.309(3)	N(1)−C(7)	1.474(6)	N(1)−C(7)	1.483(6)
N(2)−C(13)	1.520(3)	1.4622(15)	1.465(3)	N(1)−C(8)	1.479(5)	N(1)−C(8)	1.489(5)
C(8)−C(13)	1.527(3)	1.5346(16)	1.533(3)	N(3)−C(35)	1.458(5)	N(3)−C(43)	1.494(6)
C(14)−C(15)	1.507(3)	1.4604(16)	1.407(3)	N(3)−C(36)	1.486(5)	N(3)−C(44)	1.484(6)
C(6)−C(7)	1.501(3)	1.4596(16)	1.454(3)	N(2)−C(15)	1.503(6)	N(2)−C(13)	1.488(6)
				N(2)−C(22)	1.505(6)	N(2)−C(14)	1.489(6)
				N(3)−C(36)	1.486(5)	N(4)−C(49)	1.487(6)
				N(4)−C(50)	1.460(5)	N(4)−C(50)	1.487(6)
				V(1)−O(1)	1.832(3)	V(1)−O(1)	1.836(3)
				V(1)−O(2)	1.906(3)	V(1)−O(2)	1.904(3)
				V(1)−O(3)	1.622(3)	V(1)−O(3)	1.627(3)
				V(1)−O(7)	1.840(3)	V(1)−O(7)	1.843(3)
				V(1)−N(1)	2.275(4)	V(1)−N(1)	2.278(4)
				V(1)−N(2)	2.153(4)	V(1)−N(2)	2.146(4)
				V(2)−O(4)	1.850(3)	V(2)−O(4)	1.827(3)
				V(2)−O(5)	1.936(3)	V(2)−O(5)	1.827(3)
				V(2)−O(6)	1.623(3)	V(2)−O(6)	1.836(3)
				V(2)−O(7)	1.792(3)	V(2)−O(7)	1.805(3)
				V(2)−N(3)	2.289(4)	V(2)−N(3)	2.302(4)
				V(2)−N(4)	2.141(4)	V(2)−N(4)	2.132(4)
				Bond Angles			
N(1)−C(8)−C(13)	109.57(19)	108.55(9)	109.71(19)			N(1)−C(8)−C(13)	108.1(4)
N(1)−C(8)−C(9)	109.09(17)	110.37(9)	107.93(18)			N(1)−C(8)−C(9)	113.9(4)
N(1)−C(7)−C(6)	111.24(17)	121.97(11)	121.3(2)			N(1)−C(7)−C(6)	114.2(4)
N(2)−C(14)−C(15)	109.89(19)	123.07(11)	124.3(2)			N(2)−C(14)−C(15)	113.4(4)
C(13)−C(8)−C(9)	110.73(18)	110.50(10)	110.17(19)			C(13)−C(8)−C(9)	110.6(4)
C(8)−C(13)−C(12)	111.7(2)	110.56(10)	111.5(2)			C(8)−C(13)−C(12)	110.8(4)
N(2)−C(13)−C(8)	112.35(17)	108.45(9)	110.72(18)			N(2)−C(13)−C(8)	107.5(3)
N(2)−C(13)−C(12)	108.71(17)	110.79(9)	110.23(19)			N(2)−C(13)−C(12)	112.8(4)
C(14)−N(2)−C(13)	117.32(19)	118.01(10)	123.6(2)	C(35)−N(3)−C(36)	111.8(3)	C(14)−N(2)−C(13)	114.8(3)
C(7)−N(1)−C(8)	115.21(19)	118.23(10)	119.4(2)	C(7)−N(1)−C(8)	110.8(4)	C(7)−N(1)−C(8)	111.5(3)
				C(15)−N(2)−C(22)	112.0(4)	C(13)−N(2)−C(14)	114.8(3)
				O(3)−V(1)−O(1)	105.19(16)	O(3)−V(1)−O(1)	103.50(15)
				O(3)−V(1)−O(7)	97.96(15)	O(3)−V(1)−O(7)	97.37(15)
				O(1)−V(1)−O(7)	95.90(15)	O(1)−V(1)−O(7)	97.01(14)
				O(3)−V(1)−O(2)	96.66(16)	O(3)−V(1)−O(2)	95.46(14)
				O(1)−V(1)−O(2)	93.08(15)	O(1)−V(1)−O(2)	94.44(13)
				O(7)−V(1)−O(2)	160.19(14)	O(7)−V(1)−O(2)	160.31(13)
				O(3)−V(1)−N(2)	92.74(15)	O(3)−V(1)−N(2)	95.14(15)
				O(1)−V(1)−N(2)	161.74(15)	O(1)−V(1)−N(2)	161.05(14)
				O(7)−V(1)−N(2)	84.75(14)	O(7)−V(1)−N(2)	83.77(13)
				O(2)−V(1)−N(2)	81.27(15)	O(2)−V(1)−N(2)	80.25(13)
				O(3)−V(1)−N(1)	169.59(15)	O(3)−V(1)−N(1)	172.75(14)
				O(1)−V(1)−N(1)	85.21(14)	O(1)−V(1)−N(1)	83.75(13)
				O(7)−V(1)−N(1)	81.13(14)	O(7)−V(1)−N(1)	81.34(13)
				O(2)−V(1)−N(1)	82.07(14)	O(2)−V(1)−N(1)	84.05(13)
				N(2)−V(1)−N(1)	76.85(13)	N(2)−V(1)−N(1)	77.63(13)
				C(1)−O(1)−V(1)	136.9(3)	C(1)−O(1)−V(1)	139.1(3)
				C(7)−N(1)−V(1)	114.3(3)	C(7)−N(1)−V(1)	112.3(3)
				C(8)−N(1)−V(1)	109.2(3)	C(8)−N(1)−V(1)	108.8(3)
				C(15)−N(2)−V(1)	112.1(3)	C(13)−N(2)−V(1)	112.5(3)
				C(22)−N(2)−V(1)	112.3(3)	C(14)−N(2)−V(1)	111.3(3)

the existence of V═O···V═O interactions: the binding of an O_{oxo} to an adjacent vanadium, trans to its vanadyl O atom, lengthens and weakens the bond, thereby lowering the V═O stretching frequency. This is also in agreement with the EPR spectra, which in some cases denote partial aggregation if the samples are frozen immediately after dissolution of the complexes in DMSO. The FTIR spectra of the V^V complexes show only the presence of one band assigned to ν(V═O) at ca. 910 cm^{-1}, in agreement with the molecular structures determined by X-ray diffraction and the formulation assigned to **13**. The Schiff base complexes show ν(C═N) bands at ca. 1605−1625 cm^{-1}, and the ν(C−O) bands show up in the range 1150−1270 cm^{-1}.

Magnetic Properties. The magnetic susceptibilities were measured by the Faraday method at 5*T* for V^{IV}O{sal(*R*,*R*-chan)} (**7**) and V^{IV}O{sal(*S*,*S*-dpan)} (**8**) in the range 4−300 K. The variation of the μ_{eff} values with *T* and the magnetic susceptibility curves are shown in SI-3 (Supporting Information). For complex **8**, from the plot of the reciprocal paramagnetic susceptibility as a function of *T* (Curie−Weiss plot), the TIP = 1.28 × 10^{-4} emu mol^{-1} and θ = 10 K values were obtained, as well as μ_{eff} values in the range

Table 4. Selected IR Frequencies and Spin Hamiltonian Parameters Calculated by Simulation of the Experimental EPR Spectra Using the Program of Rockenbauer and Korecz[24]

	FTIR	EPR			
compound	ν(V=O) cm^{-1}	g_x, g_y (or $g_\perp$)	A_x, A_y (or $A_\perp$) $\times$ 10^4 cm^{-1}	g_z (or $g_\parallel$)	A_z (or $A_\parallel$) $\times$ 10^4 cm^{-1}
$V^{IV}O${sal(chen)} **7a**[a]	990	1.983	50.5	1.959	157.4
$V^{IV}O${sal(chan)} **7**[a]	879	1.976	50.9	1.957	158.3
$V^{IV}O${sal(dpen)} **8a**[a]	983	1.978	53.7	1.955	160.0
$V^{IV}O${sal(dpan)} **8**[a]	882	1.978	54.1	1.954	161.8
$V^{IV}O${Etvan(chen)}**9a** [b]	990	1.981, 1.983	50.7, 58.7	1.956	164.1
$V^{IV}O${Etvan(chan)}**9** [b]	842	1.978	53.3	1.955	161.7
$V^{IV}O${mvan(chen)} **10a**[b]	977	1.982	55.1	1.955	164.4
$V^{IV}O${mvan(chan)} **10**[b]	845	1.983, 1.976	55.6,52.6	1.954	160.1
$V^{IV}O${naph(chan)} **11**[a]	962	1.982, 1.976	59.8, 50.9	1.955	161.1
$V^{IV}O${*t*-Busal(chan)} **12**[b]	879	1.976, 1.982	49.1,55.9	1.955	160.8
{$V^{V}O$[sal(chan)]}$_2$(μ-O) **13**	920				
{$V^{V}O$[sal(dpan)]}$_2$(μ-O) **14c**	927				
{$V^{V}O$[*t*-Bu-sal(chan)]}$_2$(μ-O) **15c**	912				

[a] EPR spectrum measured in DMSO. [b] EPR spectrum measured in DMF.

1.67−1.85 μ_B from 90−300 K. The ν(V=O) values of 882 and 879 cm^{-1} obtained for **8** and **7**, respectively, indicate some interaction of the V=O units, possibly of the type V=O···V=O···V=O. The magnetic measurements indicate that these interactions are not strong enough to change the μ_{eff} values significantly in the case of **8**, the compound behaving as monomeric units, as long as magnetic interactions are concerned.

Crystal Structures. From two solutions containing complexes **8** and **12** dissolved in a mixture of CH_2Cl_2 and isopropanol, which were left in the air for a few weeks, dark crystals were obtained and characterized by single-crystal X-ray diffraction. Although the two molecules have quite different steric and electronic properties, they show very similar dinuclear structures in the solid state. Complex **15c** has bulky electron-donating groups in the aromatic rings (*t*-Bu) and a flexible diaminocyclohexane skeleton; **14c** has no substituents in the aromatic rings and has a diphenylethylenediamine backbone, with its steric demands. In the molecular structures, each dinuclear molecule has a μ-oxo bridge between the V^V atoms, and to our knowledge, these are the first examples of {$OV^V(\mu$-O)V^VO} neutral dinuclear μ-oxo-bridged V^V species with tetradentate dianionic ligands. Most {$OV^V(\mu$-O)V^VO} units reported are formed from tridentate ligands.[38−44] Moreover, the examples found in the literature with tetradentate ligands are mixed-valence V(IV/V) dimers.[45−47] Also, both structures present twist-angular configurations and phenolate oxygen atoms cis-oriented to each other (cis-β-type structures).

[{V^VO[sal(*S*,*S*-dpan)]}$_2$(μ-O)]·2H_2O·3.5$(CH_3)_2CHOH$ (14c). The V^V compound formed upon the slow oxidation and dimerization of the $V^{IV}O$ complex that was probably driven by the electron deficiency and oxophilicity of the V^V ion. The asymmetric unit contains two formula units of [{V^VO[sal(*S*,*S*-dpan)]}$_2$(μ-O)], as well as two water and 3.5 isopropanol molecules.

Figure 2 shows a representation of one of the [{V^VO-[sal(*S*,*S*-dpan)]}$_2$(μ-O)] units with the atom-labeling scheme. Table 3 contains selected bond lengths and angles, and section SI-2 (Supporting Information) gives some additional X-ray data.

In the molecular structures, the vanadium center adopts a distorted six-coordinate octahedral geometry with the sal(dpan) ligand coordinated through the two $O_{phenolate}$ and two N_{amine} atoms; the oxo and bridging μ-oxo atoms complete the coordination sphere. The phenolate O atoms are cis-oriented to each other (cis-β-type structure) in both molecules of the unit cell. The vanadium atom in each core is displaced toward the apical oxo ligand from the equatorial plane defined by the two $O_{phenolate}$, one N_{amine}, and μ-oxo atoms by less than 0.074 Å.

The four V=O bonds are very similar (average: 1.621(6) Å) and characteristic of oxo-type O atoms with strong π bonding. The torsion angles of the planes containing V1−O3, V2−O7, V3−O10, and V4−O13 bonds (O2−O3−O7−N1, O5−O6−O7−N3, O9−O10−014−N5, and O12−O13−O14−N7, respectively) are 92.6° and 82.5°, corresponding to twist-angular configurations.[49] The V−μ-oxo bonds also show π-bonding character, but to a lesser extent, presenting an average length of 1.82(6) Å. The V−$O_{phenolate}$ bonds, which are trans to the μ-oxo atoms, are significantly longer (average: 1.91(4) Å) than those that are trans to the N_{amine} atoms (average length: 1.85(3) Å). The same trans effect is also seen in the V−N_{amine} bonds, which are longer when trans to the V=O bond (2.15(2) vs 2.29(2) Å). The V−V

(38) Carrano, C. J.; Nunn, C. M.; Quan, R.; Bonadies, J. A.; Pecoraro, V. L. *Inorg. Chem.* **1990**, *29*, 944–951.
(39) Dutta, S.; Basu, P.; Chakravorty, A. *Inorg. Chem.* **1993**, *32*, 5343–5348.
(40) Dai, J.; Akiyama, S.; Munakata, M.; Mikuriya, M. *Polyhedron* **1994**, *13*, 2495–2499.
(41) Cavaco, I.; Costa Pessoa, J.; Duarte, M. T.; Henriques, R. T.; Matias, P. M.; Gillard, R. D. *J. Chem. Soc., Dalton Trans.* **1996**, 1989–1996.
(42) Schmidt, H.; Bashirpoor, M.; Rehder, D. *J. Chem. Soc., Dalton Trans.* **1996**, 3865–3870.
(43) Sangeetha, N. R.; Pal, S. *Bull. Chem. Soc. Jpn.* **2000**, *73*, 357–363.
(44) Diamantis, A. A.; Frederiksen, J. M.; Salam, M. A.; Snow, M. R.; Tiekink, E. R. T. *Aust. J. Chem.* **1986**, *39*, 1081–1088.
(45) Kojima, A.; Okazaki, K.; Ooi, S.; Saito, K. *Inorg. Chem.* **1983**, *22*, 1168–1174.
(46) Launay, J. P.; Jeannin, Y.; Daoudi, M. *Inorg. Chem.* **1985**, *24*, 1052–1059.
(47) Mahroof-Tahir, M.; Keramidas, A. D.; Goldfarb, R. B.; Anderson, O. P.; Miller, M. M.; Crans, D. C. *Inorg. Chem.* **1997**, *36*, 1657–1668.
(48) Desiraju, G. R.; Steiner, T. *The Weak Hydrogen Bond in Structural Chemistry and Biology*; Oxford University Press: Oxford, U. K., 1999.
(49) Dutta, S. K.; Samanta, S.; Kumar, S. B.; Han, O. H.; Burckel, P.; Pinkerton, A. A.; Chaudhury, M. *Inorg. Chem.* **1999**, *38*, 1982–1988.

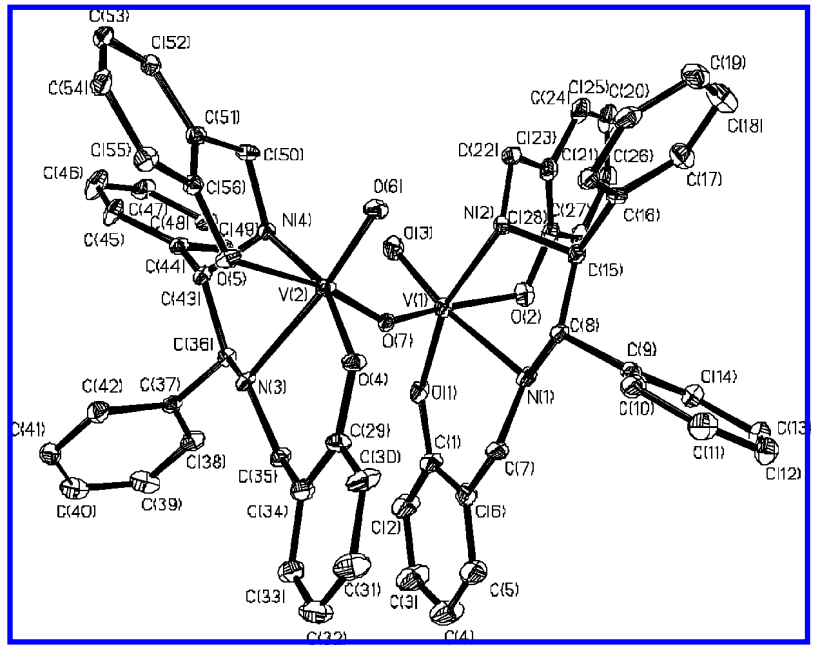

Figure 2. ORTEP diagram of one of the $[\{V^{V}O[sal(S,S\text{-dpan})]\}_2(\mu\text{-O})]$ units of **14c** with the atom-labeling scheme, with the thermal ellipsoids of the non-hydrogen atoms drawn at the 30% probability level. The hydrogen atoms and solvent molecules were omitted for clarity.

separation is 3.525 and 3.492 Å in the two dinuclear units, and the V−μ-oxo−V angles are 152.04(19)° (V1−O7−V2) and 146.37(17)° (V3−O14−V4).

Most of the important H-bonds in **14c** are either intramolecular or intermolecular hydrogen bonds between the units of $[\{V^{V}O[sal(S,S\text{-dpan})]\}_2(\mu\text{-O})]$ and the solvent molecules. However, H-bonds between the two parts of the dinuclear units exist, but they are weak[48] (see section SI-2, Supporting Information).

$[\{V^{V}O[t\text{-Busal}(R,R\text{-chan})]\}_2(\mu\text{-O})]\cdot 2(CH_3)_2CHOH$ (15c). The **15c** molecule contains the dinuclear unit $[\{V^{V}O[t\text{-Bu-sal}(R,R\text{-chan})]\}_2(\mu\text{-O})]$, derived from 3,5-di-*tert*-butylsalicylaldehyde and 1*R*,2*R*-diaminocyclohexane. The asymmetric unit contains one $[\{V^{V}O[t\text{-Bu-sal}(R,R\text{-chan})]\}_2(\mu\text{-O})]$ dimer. Each vanadium atom is surrounded by a distorted octahedron formed by the oxo O atom, the bridging O atom, and the four coordinated ONNO atoms of the *t*-Busal(chan) ligand (see Figure 3). The tetragonal planes are best defined by O4−O5−O7−N4 (mean deviation from plane = 0.0233 Å) and O1−O2−O7−N1 (mean deviation from plane = 0.0489 Å), leaving the oxo atoms (O3 and O6) and the other N atoms, N1 and N3, in the axial positions. The torsion angles of the planes containing V1−O3 and V2−O7 bonds (O2−O3−O7−N1 and O4−O6−O7−N3, respectively) are 89.4°, corresponding to a twist-angular configuration,[49] similarly to **14c**.

Once again, the $O_{phenolate}$ atoms are cis-oriented to each other (cis-β structures). The axial V−N_{amine} distances are rather long, for example, V1−N1 = 2.278(4) Å and V1−N3 = 2.302(4) Å, due to the trans influence of the oxo atoms, and are longer than the equatorial V−N_{amine} distances: {e.g. V1−N2 = 2.146(4) Å, V2−N4 = 2.132(4) Å}. As in **14c**, the two V centers are not equivalent, and the V−O−V bridge is slightly asymmetric {V1−O7 = 1.843(3) Å, V2−O7 = 1.805(3) Å}, the bridging angle V1−O7−V2 being 150.50(18)°.

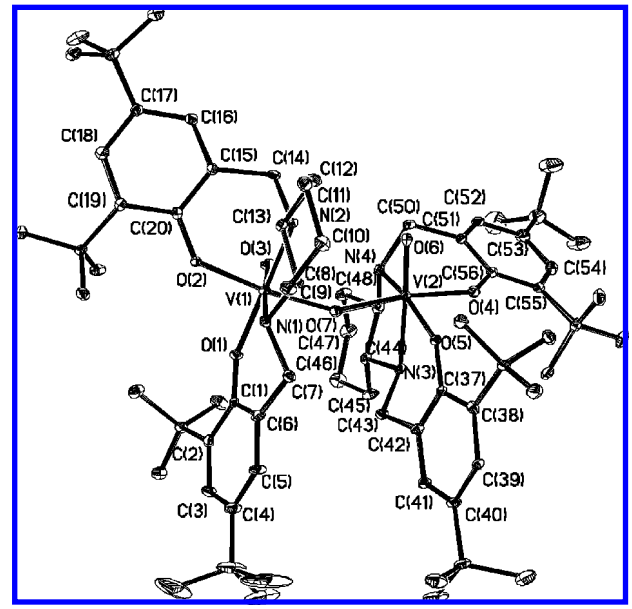

Figure 3. ORTEP diagram of one of the $[\{V^{V}O[t\text{-Busal}(R,R\text{-chan})]\}_2(\mu\text{-O})]$ units of **15c** with the atom-labeling scheme, with the thermal ellipsoids of the non-hydrogen atoms drawn at the 30% probability level. The hydrogen atoms and solvent molecules have been omitted for clarity.

Hydrogen bonds exist between the two parts of the dinuclear units (N_{amine}−$O_{terminal}$, N2−H2···O6, and N4−H4···O3), slightly stronger than those found in **14c**,[48] and between the $[V^{V}O\{sal(dpan)\}_2(\mu\text{-O})]$ units and the solvent molecules (see section SI-2, Supporting Information).

Solution Characterization. The solutions of the $V^{IV}O$−salan complexes are not stable to oxidation. When dissolved in organic solvents (DMSO, DCM, MeCN, MeOH, and DCE = 1,2-dichloroethane), their solutions change with time. In this section, we present the characterization of the $V^{IV}O$−salen complexes and the study of the oxidation of the $V^{IV}O$−salan complexes (by spectroscopic techniques).

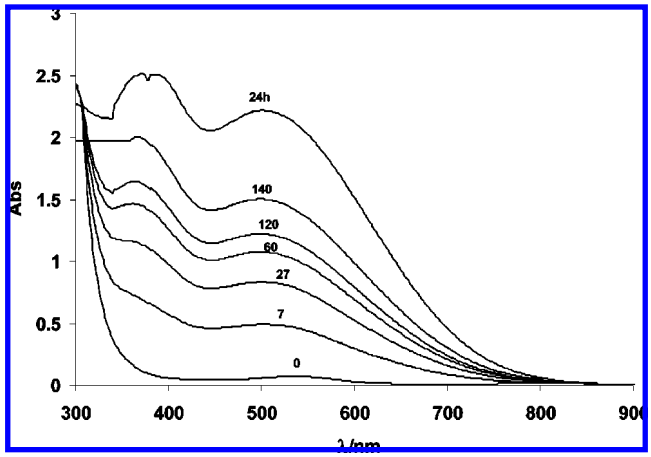

Figure 4. Change with time of the UV−vis spectra for solutions containing complex **7** (0.3 mM) in DMSO. Time (in minutes, except when indicated) is indicated for each spectrum.

Electronic Absorption Spectra. The $V^{IV}O$−salen complexes **7a**−**10a** present two weak d−d bands in the visible region at ca. 660−800 nm (band I, $d_{xy} \rightarrow d_{xz}$, d_{yz}) and 520−600 nm (band II, $d_{xy} \rightarrow d_{x^2-y^2}$). The third expected transition ($d_{xy} \rightarrow d_{z^2}$) is not always distinguishable since it is below 400 nm, under a strong CT band.[50] The $V^{IV}O$−salan complexes, immediately after dissolution, show d−d bands at ca. 550−600 nm, and a shoulder or distinct band may appear at 750−800 nm. With time, these solutions turn strong red-brown. Figure 4 shows the changes with time of the UV−vis spectra for a 0.3 mM solution of complex **7** dissolved in DMSO. The initial spectrum at $t = 0$ corresponds to a typical spectrum of a $V^{IV}O$ complex, showing two bands in the visible region, one at $\lambda_{max} \sim 800$ nm and another at 530 nm, which may be attributed to bands I ($d_{xy} \rightarrow d_{xz}$, d_{yz}) and II ($d_{xy} \rightarrow d_{x^2-y^2}$), respectively.[50]

With time, the intensity of the band at ca. 530 nm increases, and its maximum shifts to higher energy. A new band also develops at ca. 370 nm (final $\varepsilon = 8350\ M^{-1}\ cm^{-1}$), and 24 h later, the equilibrium is reached and the lower energy band has $\lambda_{max} = 498$ nm ($\varepsilon = 7380\ M^{-1}\ cm^{-1}$). The bands that form have high extinction coefficients and cannot be assigned to d−d transitions. The transition at 500 nm in Figure 4 in solutions containing V^V complexes is probably a charge transfer from a $p\pi$ orbital on the phenolate oxygen lone pair to the empty 3d orbitals of the vanadium atom.[51] The other strong band (at 370 nm) is also attributed to the phenolate-bound vanadium(V) species; this is consistent with the two ligand-to-metal charge transfer (LMCT) transition ranges of 320−380 and 475−550 nm reported for several oxovanadium(V) complexes.[52] Therefore, the V^{IV} is being oxidized by molecular oxygen into a V^V species. It is possible that a V^VO^{3+} complex may form at the initial stages of the oxidation, but in the ^{51}V NMR spectrum after 4 h of dissolution, a single peak is clearly detected (at −551 ppm in DMSO) that we assign to the formation of a VO_2−sal(chan) complex (see below).

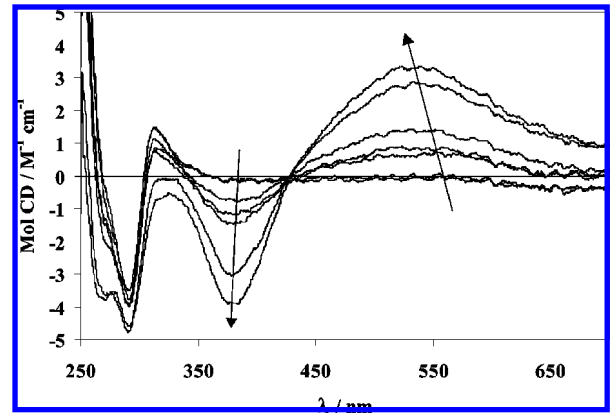

Figure 5. Variation of the CD spectra with time (0−75 min) for solutions containing complex **7** (0.3 mM) in DMSO.

Circular Dichroism. Figure SI-4-2 (Supporting Information) shows CD spectra of solutions of V^{IV}−salan compounds **7** and **8**, and of V^{IV}−salen complexes **7a** and **8a** in DMSO. The electronic d−d transitions in the visible region are very weak for the V^{IV}−salan compounds, and the CD signal is also very weak in this wavelength range. As the V^{IV}−salan complexes oxidize very easily, special care must be taken since small amounts of a V^V complex produce a much more intense LMCT band (see below). CD spectra of solid samples in KBr disks or Nujol mulls of several V^{IV}−salan complexes were also recorded, preparing the samples as described previously,[53] but the signals were extremely weak in the 450−1000 nm range and do not allow reliable comparisons between the different complexes.

Figure 5 presents the change of the CD spectra with time for solutions containing complex **7**. The initial spectrum ($t = 0$ min) for $\lambda > 350$ nm shows only low-intensity bands, as normally found for $V^{IV}O$ complexes in the visible region, since these bands are due to d−d transitions. Below ca. 350 nm, bands show up at 289 ($\Delta\varepsilon = -3.2\ M^{-1}\ cm^{-1}$) and 310 nm ($\Delta\varepsilon = 1.3\ M^{-1}\ cm^{-1}$). With time, a broad positive band develops at ca. 530 nm and another one of negative sign at ca. 375 nm. The changes observed are in agreement with the data from the UV−vis absorption spectra (Figure 4), and the new bands should be due to CT transitions from the new V^V species being formed.

EPR. The X-band EPR spectra of frozen solutions (77 K) of the vanadium complexes dissolved in DMSO were measured and simulated (whenever possible) with a computer program from Rockenbauer and Korecz[24] (see Table 4). For the $V^{IV}O$−salan complexes, the spectra are either axial or show a small rhombic distortion. With $V^{IV}O$−pyran complexes [pyran = N,N′-ethylene-bis(pyridoxylaminato)] in aqueous solution, two distinct types of complexes could be clearly detected by EPR,[7] corresponding to structural isomers (one with H_2O coordinated in the equatorial position, and the other with all donor atoms of the pyran ligand bound

(50) Vilas Boas, L. F.; Costa Pessoa, J. *Comprehensive Coordination Chemistry*; Wilkinson, G., Gillard, R. D., McCleverty, J. A., Eds.; Pergamon Press: Oxford, U. K., 1987; Vol. 3, pp 453−583.
(51) Bhattacharya, S.; Ghosh, T. *Trans. Met. Chem.* **2002**, *27*, 89–94.
(52) Ghosh, T.; Bhattacharya, S.; Das, A.; Mukherjee, G.; Drew, M. G. B. *Inorg. Chim. Acta* **2005**, *358*, 989–996.
(53) Costa Pessoa, J.; Calhorda, M. J.; Cavaco, I.; Correia, I.; Duarte, M. T.; Felix, V.; Henriques, R. T.; Piedade, M. F. M.; Tomaz, I. *J. Chem. Soc., Dalton Trans.* **2002**, 4407–4415.

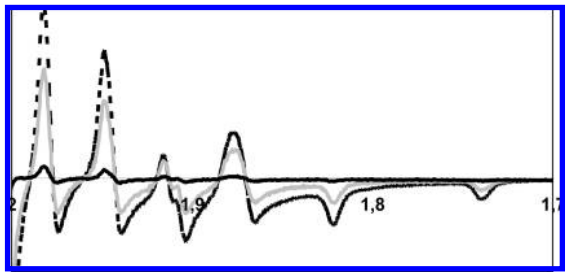

Figure 6. High-field region of the EPR spectra of **7** in DMSO (10 mM) showing an overlay of the signals for several time intervals: $t = 15$ min (---), 1 h (gray —), and 4 h (black —); $t = 0$ corresponds to the dissolution of the sample.

equatorially). However, for all complexes reported here, the pattern of the EPR spectra is compatible with only one type of V^{IV}−salan species being present.

Three binding modes are possible with these chelates, if we consider an octahedral geometry with a solvent molecule coordinated: either the solvent is coordinated trans to the oxo group, or one O or N atom occupies this position. There are other isomers for these structures, but they are not distinguishable by EPR. For the $V^{IV}O$−salan complexes, the values obtained for the hyperfine coupling constant are within $158.3 \times 10^{-4} \leq A_{\parallel} \leq 161.8 \times 10^{-4}$ cm^{-1}. The three possible binding modes $(2 \times N_{amine}, 2 \times O_{phenolate})_{eq}$, $(2 \times O_{phenolate}, N_{amine}, DMSO)_{eq}(N_{amine})_{ax}$, and $(O_{phenolate}, 2 \times N_{amine}, DMSO)_{eq}(O_{phenolate})_{ax}$ have $A_{\parallel}^{est}$[25,26] values of 157×10^{-4}, 159×10^{-4}, and 161×10^{-4} cm^{-1}, respectively, considering the following contributions: $A_{i,amine} = 40.1 \times 10^{-4}$ cm^{-1} and $A_{i,phenolate} = 38.9 \times 10^{-4}$ cm^{-1}. Since the estimated accuracy of $A_{\parallel}^{est}$ is 3×10^{-4} cm^{-1},[25] no binding mode can be assigned with certainty. For the V^{IV}−salen complexes **7a** and **8a**, the most probable binding mode is $(2 \times O_{phenolate}, 2 \times N_{imine})_{eq}$, which has the lowest $A_{\parallel}^{est}$ value (ca. 158×10^{-4} cm^{-1}). For compounds **9a** and **10a** in DMF, the A_z values are significantly higher, being consistent with a binding mode with one DMF molecule bound equatorially.

The oxidation of the $V^{IV}O$−salan complexes was also followed using EPR. Complex **7** was dissolved in DMSO (ca.10 mM), and the solution was left in the air. EPR samples were taken at different time intervals: 15 min and 1 and 4 h, the samples being immediately frozen, and the spectra were measured at 77 K, with constant acquisition parameters. The intensity of the central lines of the EPR spectra progressively decreases with time, confirming that the complex is being oxidized. In Figure 6, where an overlay of the EPR lines in the high-field region is shown, we can also observe that the $V^{IV}O$ species present in solution, as the oxidation proceeds, is the same, since the positions of the EPR lines do not change. For complex **8**, a similar behavior was observed.

^{51}V NMR. Table 5 contains the data concerning the ^{51}V NMR characterization of the V^{V} complexes, which were measured in different solvents. Complex **13** shows one peak at ca. −546 ppm in CH_2Cl_2 and DMSO. In MeCN, besides a peak at −551 ppm, two smaller ones are also observed, which probably correspond to different coordination isomers. The only two monomeric V^{V}−salan complexes so far characterized by X-ray diffraction[7,8] are two $V^{V}O_2$−pyran-type compounds, and in aqueous solution, two types of isomers were always detected in the ^{51}V NMR spectra: (i) for α-cis isomers depending on pH signals between −563 and −577 ppm and (ii) for β-cis isomers with signals between −544 and −563 ppm, also depending on pH. Therefore, we assign the resonances at ca. −550 ppm to VO_2L-type complexes. When dissolved in MeOH, complex **13** shows only a downfield resonance at −487 ppm. This peak is assigned to a [VOL(CH_3OH)]-type complex. Coordination of methanol increases the metal shielding and hence shifts the resonance to less negative values.[54,55] Complexes **14c** and **15c**, also characterized by X-ray diffraction, are dinuclear in the solid state. However, in solution, the dinuclear structure is probably disrupted, and monomeric complexes are formed: **14c** and **15c** show only one peak in CD_2Cl_2 at −557 and −550 ppm, respectively. This is the region assigned to [VO_2L] complexes.[56] In MeOD, another peak is observed downfield, at −501 and −499 ppm for **14c** and **15c**, respectively. This deshielded peak is also assigned to a complex with a coordinated methanol molecule: [VOL(CH_3OH)] (see section SI-6, Supporting Information).

The oxidation of the $V^{IV}O$−salan complexes was also studied by ^{51}V NMR. The complexes were dissolved in the organic solvents and left in the air for different periods of time, after which the spectra were measured. For complexes **7** and **8** in DMSO (ca. 7 mM) after 4 h, the ^{51}V NMR spectra showed broad signals (W1/2 ∼ 3700 Hz) at −551 ppm (**7**) and −537 ppm (**8**) (see Table 5). For the same solutions, EPR spectra could be recorded (e.g., Figure 6), the V^{IV} complexes contributing to the broadening of the peaks detected. When dissolved in CH_2Cl_2 under similar conditions, complexes **7** and **8** present narrower peaks (W1/2 ∼ 1000 Hz) at −540 and −549 ppm, respectively. The broadness of the resonances in DMSO is probably due to the higher viscosity of this solvent when compared to CH_2Cl_2 and the formation of several isomers of the V^{V} species. We assign these peaks to [VO_2L] complexes. When **7** is dissolved in methanol in the presence of air, after ca. 4 h, a peak is detected at −488 ppm, probably due to the formation of the complex with a coordinated methanol (after 24 h, a very weak signal is also detected at −543 ppm). In some cases, for example, compounds **9**, **10**, and **11**, the oxidation process took several days. Five days after the dissolution of the V^{IV} compounds in DCE, several peaks were detected in the ^{51}V NMR spectra of the three compounds. With **12**, after 1 h, several peaks were detected, but after 5 days, only one signal was found at −549 ppm.

The chemical shifts reported in Table 5 are not decisive in establishing which type of species form, namely, between $V^{V}O$, $V^{V}O_2$ and $V^{V}_2O_3$−salan compounds. Formation of

(54) Choudhary, N. F.; Hitchcock, P. B.; Leigh, G. J. *Inorg. Chim. Acta* **2000**, *310*, 10–20.
(55) Fairhurst, S. A.; Hughes, D. L.; Kleinkes, U.; Leigh, G. J.; Sanders, J. R.; Weisner, J. *J. Chem. Soc., Dalton Trans.* **1995**, 321–326.
(56) (a) Maurya, M. R.; Agarwal, S.; Abid, M.; Azam, A.; Bader, C.; Ebel, M.; Rehder, D. *Dalton Trans.* **2006**, 937–947. (b) Nica, S.; Rudolph, M.; Gorls, H.; Plass, W. *Inorg. Chim. Acta* **2007**, *360*, 1743–1752. (c) Maurya, M. R.; Agarwal, S.; Bader, C.; Ebel, M.; Rehder, D. *Dalton Trans.* **2005**, 537–544. (d) Maurya, M. R.; Khurana, S.; Zhang, W.; Rehder, D. *J. Chem. Soc., Dalton Trans.* **2002**, 3015–3023.

Table 5. ^{51}V NMR Parameters for the Oxidized Solutions of the $V^{IV}O$ Complexes and for the V^{V} Complexes **13**, **14c**, and **15c**

compound	solvent	time	H_2O_2 (eq)	δ (ppm)
$V^{IV}O$\{sal(chen)\} **7a**	CH_3OH		0.5	−570
	CH_3OH		1.5	−645, −667
$V^{IV}O$\{sal(chan)\} **7**	CH_2Cl_2	4 h		−540
	DCE	1 day		−548
	DMSO	4 h		−551 (br)
	CH_3CN	3 h		−536 (5%), −551 (90%), −565 (5%)
			4.5	−511, −551, −585, −644
	CH_3OH	1 day		−488 (>95%), −543
			2	−488 (60%), −648 (40%)
			5	−488 (20%), −648 (80%)
$V^{IV}O$\{sal(dpan)\} **8**	CH_2Cl_2	4 h		−549
	DMSO	4 h		−537 (br)
$V^{IV}O$\{Etvan(chan)\} **9**	DCE	5 days		−493, −530, −550, −625, −642
$V^{IV}O$\{mvan(chan)\} **10**	DCE	5 days		−442, −450, −479, −484, −527, −549, −645
$V^{IV}O$\{naph(chan)\} **11**	DCE	5 days		−473, −538, −639
$V^{IV}O$\{*t*-Busal(chan)\} **12**	DCE	1 h		−472, −506, −528, −546, −669
	DCE	5 days		−549
$\{V^{V}O$[sal(chan)]$\}_2(\mu$-O) **13**	CH_2Cl_2			−546
	CH_3CN			−537 (5%), −551 (90%), −565 (5%)
	CH_3OH			−487
$\{V^{V}O$[sal(dpan)]$\}_2(\mu$-O) **14c**	MeOD			−501, −549
	CD_2Cl_2			−557
$\{V^{V}O$[*t*-Busal(chan)]$\}_2(\mu$-O) **15c**	MeOD			−499, −555
	CD_2Cl_2			−550

mixed-valence $V^{IV}-O-V^{V}$ species[57] probably would not be detected in ^{51}V NMR. However, for the present V^{V} species formed upon the oxidation of V^{IV} complexes, the ligands being flexible and potentially tetradentate, we do not expect $V^{V}O$ complexes to be very stable. If they form at the initial stage of the oxidation, with time and contact with moisture, they probably yield $V^{V}O_2$ or $V^{V}{}_2O_3$−salan compounds. By comparison with the V^{V}−pyran complexes and other complexes with N,O donor sets,[56] we assign the peaks in the range ca. −525 to −550 ppm to the formation of $V^{V}O_2$−salan compounds and those in the range ca. −480 to −525 ppm to $V^{V}O$ species with the solvent coordinated.

The differences observed in the $\delta(^{51}V)$ values with varying solvents (see Table 5) can be explained by solvation effects. A linear solvation energy relationship (LSER) analysis with the Kamlet−Taft[58] parameters of the solvents and the chemical shift of complex **7** (in five solvents) was done. Each of the parameters is empirically obtained and has been measured for a wide range of solvents.[59] These scales have been used in multiparameter equations to fit a number of different solvent-dependent observations, with the most useful form shown in eq 1:

$$\delta(^{51}V) = XYZ_0 + a\alpha + b\beta + s\pi^* \qquad (1)$$

where XYZ_0 is the $\delta(^{51}V)$ without any solvent effect, α is a quantitative scale of the hydrogen-bond acidity of a solvent or its ability to donate a hydrogen bond, β is a scale of the hydrogen-bond basicity of a solvent or its ability to accept a hydrogen bond, and π^* is the solvent dipolarity/polarizability, which is a scale of the ability of the solvent to stabilize a charge or dipole. The error associated with each parameter of eq 1 was appraised in terms of the p value, and any terms found to be statistically insignificant were eliminated. It was decided to take as acceptable only those parameters whose statistical significance p value does not exceed the limit level of 0.05. Figure 7 shows the correlation and includes the statistical parameters obtained for eq 1a. There is an excellent correlation ($r^2 = 0.998$) containing the three parameters α, β,and π^* (see SI-5 for details, Supporting Information):

$$\delta(^{51}V) = -584(3) + 17.3(8)\alpha - 18.7(9)\beta + 48(3)\pi^* \qquad (1a)$$

We can conclude that the solvation effect is very complex, since all parameters have a strong influence, with the dipolarity/polarizability of the solvent being the most important.

Reactivity. The spectroscopic studies presented above show that the $V^{IV}O$−salan complexes are readily oxidized upon dissolution in the air. The addition of H_2O_2 accelerates the process, and it was observed that the addition of sodium dithionite reverts the equilibrium to the initial $V^{IV}O$ species.

One hour after the dissolution of complex **7** in MeOH, the UV−vis spectrum shows several bands assigned to a V^{V} species: two LMCT bands at 494 and 330 nm, as well as two other bands in the UV that are ligand-based. In the ^{51}V NMR spectrum (measured after 1 day), two peaks are observed at −488 ppm (95%) and −547 ppm (5%) [assigned to $V^{V}OL(MeOH)$ and $V^{V}O_2L$]. Upon the addition of a large excess of H_2O_2, the LMCT bands disappear and the spectra lose intensity, the final spectrum being similar to that of the free ligand (λ_{max} = 272 nm). The ^{51}V NMR spectrum measured after the addition of 2 equiv of H_2O_2 to the oxidized solution shows the appearance of a new peak at −650 ppm and a decrease of the one at −488 ppm (two minor peaks are also observed at −672 and −624 ppm; see SI-6,

(57) Tsuchida, E.; Yamamoto, K.; Oyaizu, K.; Iwasaki, N.; Anson, F. C. *Inorg. Chem.* **1994**, *33*, 1056–1063.
(58) (a) Kamlet, M. J.; Abboud, J. L.; Taft, R. W. *J. Am. Chem. Soc.* **1977**, *99*, 6027–6038. (b) Kamlet, M. J.; Taft, R. W. *J. Am. Chem. Soc.* **1976**, *98*, 377–383. (c) Taft, R. W.; Kamlet, M. J. *J. Am. Chem. Soc.* **1976**, *98*, 2886–2894. (d) Yokoyama, T.; Taft, R. W.; Kamlet, M. J. *J. Am. Chem. Soc.* **1976**, *98*, 3233–3237.
(59) Reichardt, C. *Solvents and Solvent Effects in Organic Chemistry*; Wiley-VCH: Weinheim, Germany, 2003.

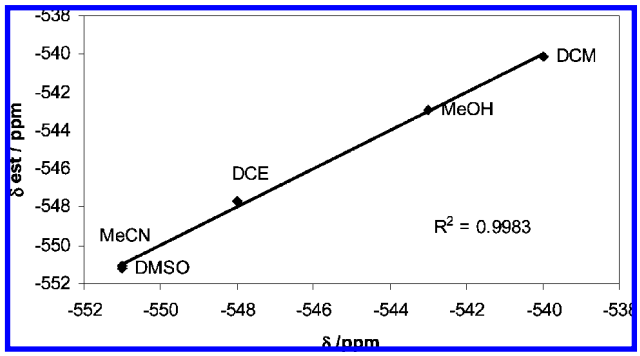

Figure 7. Kamlet−Taft LSER fit on $\delta(^{51}V)$ of complex **7**. Statistical *p* values obtained for each parameter in eq 1a: *p* value(XYZ_0) = 0.003, *p* value(*a*) = 0.03, *p* value(*b*) = 0.03 and *p* value(*s*) = 0.05 (see also section SI-5, Supporting Information).

Supporting Information). The peak at −650 ppm should correspond to an inorganic peroxovanadate, since the UV−vis spectra show that, upon the addition of H_2O_2, the ligand starts to decoordinate the vanadium center. We assign this peak to $VO(O_2)_2^-$, by comparison with literature data.[60]

In the other studied solvents (DMSO, MeCN, and DCE), the intensity of the UV−vis spectra increases considerably upon the addition of a few equivalents of H_2O_2 (up to 6 equiv) and then starts to decrease, with the formation of inorganic peroxovanadates and the decoordination of the ligand. Table 5 summarizes the data.

The solutions of the V−salen complexes are more stable to oxidation than their V−salan counterparts. However, upon the addition of 0.5 equiv of H_2O_2 to a methanolic solution of **7a**, a peak of very low intensity is observed at −570 ppm (see section SI-6, Supporting Information). This should correspond to the peroxo complex $[V^VO(O_2)(salchen)]$. With higher amounts of peroxide, only the inorganic peroxovanadates are detected. The ^1H NMR spectra of these solutions clearly show the aldehyde CHO peak and other peaks also corresponding to products of hydrolysis of the Schiff base complex and the salen ligand. In the ^1H NMR spectra of solutions of **7** after the addition of aqueous H_2O_2 solution, no peaks resulting from hydrolysis of the sal(chan) ligand were detected.

Globally, we found that, in solutions of organic solvents containing water, the V^{IV}−salan complexes are much less susceptible to hydrolysis than the corresponding the V^{IV}−salen compounds. Moreover, upon the addition of aqueous H_2O_2, the relative amount of peroxovanadates (e.g., $[VO(O_2)_2]^-$) is significantly lower in the case of the V^V−salan compounds.

When compound **13** is dissolved in methanol, only one peak is observed in the ^{51}V NMR spectrum (at −487 ppm, Figure 8). Upon the addition of H_2O_2 (1 or 2 equiv), weak signals develop at −580 ppm, probably due to the $[V^VO(O_2)(chan)]^-$ complex and at −648 ppm, assigned to $[VO(O_2)_2]^-$. The addition of 4 equiv of H_2O_2 decreases the intensity of the −487 ppm peak and strongly increases the intensity of the one at −648 ppm. We can conclude that, although the peroxo complex forms (assigned to the peak at

(60) Slebodnick, C.; Pecoraro, V. L. *Inorg. Chim. Acta* **1998**, *283*, 37–43.

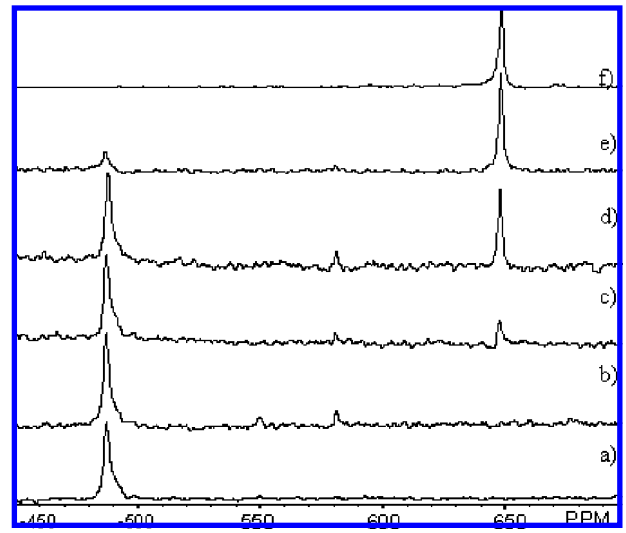

Figure 8. ^{51}V NMR spectra of complex **13** dissolved in methanol (3 mM). (a) 24 h upon dissolution; (b) after addition of 1 equiv of H_2O_2 to the previous solution; (c) addition of 2 equiv of H_2O_2; (d) addition of 4 equiv of H_2O_2; (e) addition of 10 equiv of H_2O_2; (f) addition of excess H_2O_2.

Scheme 2. Oxidation Products of Styrene by V−Salen and V−Salan Complexes **7**, **7a**, **8**, and **8a**: Phenylacetaldehyde (phaa), Benzaldehyde (bza), Benzoic Acid (bzac), and 1-Phenylethane-1,2-diol (phed)

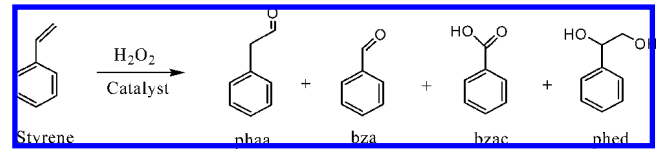

−580 ppm), most of the vanadium is converted to the inorganic peroxovanadate. This may explain the relatively low enantioselectivities observed in the asymmetric sulfoxidation reactions (see below).

Catalytic Studies. In order to screen the catalytic oxidative potential of the prepared complexes, they were applied in the oxidation of some simple organic molecules with H_2O_2. Two main types of reactions were studied: (i) oxidation of the double bonds (styrene, cumene, and cyclohexene), with no particular objective concerning steoreoselectivity of the products, acetonitrile being used as solvent, and (ii) sulfoxidation (thioanisole was used as a model compound), here with the objective of achieving stereoselective oxidation to the corresponding sulfoxide (*R*- or *S*-methyl phenyl sulfoxide). In both types of reaction, the corresponding V−salen complexes were also tested for comparison.

Oxidation of Styrene. The oxidation of styrene, catalyzed by $V^{IV}O$ complexes, was carried out in acetonitrile using 30% aqueous H_2O_2 as an oxidant to give benzaldehyde (bza), 1-phenylethane-1,2-diol (phed), benzoic acid (bzac), and phenylacetaldehyde (phaa). The formation of different products is presented in Scheme 2.

The reaction conditions were optimized using 5 mmol of styrene in 10 mL of acetonitrile, varying the temperature (50−80 °C) and the amount of catalyst (0.1, 0.2, and 0.3 mmol) and H_2O_2 (5, 10, and 15 mmol). The conversion increased with the temperature, and at 80 °C, the use of 10 mmol of aqueous 30% H_2O_2, CH_3CN (10 mL), and 0.1 mmol of the catalyst was found to be optimum for the conversion

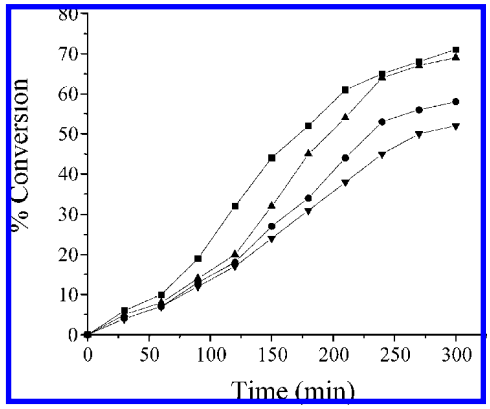

Figure 9. Oxidation of styrene catalyzed by complexes **7** (-■-), **7a** (-▲-), **8** (-●-), and **8a** (-▼-) as a function of time. Reaction conditions: styrene (0.52 g, 5 mmol), catalyst (0.1 mmol), aqueous 30% H_2O_2 (1.13 g, 10 mmol) CH_3CN (10 mL), and temperature (80 °C).

Table 6. Percent Conversion of Styrene, Turnover Frequency (h^{-1}), and Product Selectivity (See Scheme 2)

			selectivity,[a] mol %			
catalyst	conversion (%)	TOF	phaa	bza	bzac	phed
$V^{IV}O${sal(chen)} **7a**	69	6.9	12.8	58.8	21.5	6.9
$V^{IV}O${sal(dpen)} **8a**	52	5.2	1.6	91.5	5.2	1.7
$V^{IV}O${sal(chan)} **7**	71	7.1	16.3	40.6	34.4	3.7
$V^{IV}O${sal(dpan)} **8**	58	5.8	9.6	66.5	13.2	10.7

[a] phaa = Phenylacetaldehyde, bza = benzaldehyde, bzac = benzoic acid, phed = 1-phenylethane-1,2-diol. Reaction conditions as mentioned in Figure 9.

of 5 mmol of the substrate. Therefore, these reaction conditions were selected to carry out further catalytic studies.

The conversions obtained with these experimental conditions, plotted as a function of time, are presented in Figure 9. Table 6 provides details on the turnover frequency for the various catalysts and selectivity of the various products obtained at the end of 5 h of reaction.

As shown, complexes **7** [$V^{IV}O${sal(chan)}] and **7a** [$V^{IV}O${sal(chen)}] show the highest catalytic activity with ca. 70% conversion of styrene after 5 h, while **8** and **8a** gave only 58 and 52% conversion, respectively. Within the two ligand systems tested in these reactions, vanadium complexes with reduced SB ligands (V−salan) perform better than the nonreduced SB complexes (V−salen). The catalysts involving diaminocyclohexane-containing ligands are less selective for benzaldehyde than those derived from diphenylethylenediamine-containing ligands. The most commercially interesting product, styrene oxide, is not found among the reaction products, possibly because after being formed it is transformed into other products. The selectivity for benzaldehyde is the highest, and this is possibly due to the nucleophilic attack of H_2O_2 to styrene oxide, formed during the reaction, followed by cleavage of the intermediate hydroperoxystyrene. Benzaldehyde formation may also be facilitated by direct oxidative cleavage of the styrene side-chain double bond via a radical mechanism. The formation of benzoic acid through benzaldehyde oxidation is quite likely. Isomerization of styrene oxide may yield phenylacetaldehyde. The hydrolysis of styrene oxide by water present in H_2O_2 to 1-phenylethane-1,2-diol is also a plausible mechanism for the formation of this product.

Scheme 3. Oxidation Products of Cyclohexene by V−Salen and V−Salan Complexes **7**, **7a**, **8**, and **8a**: 1,2-Epoxycyclohexane (cho), Cyclohex-2-enol (chol), Cyclohex-2-enone (chone), and Cyclohexane-1,2-diol (chdol)

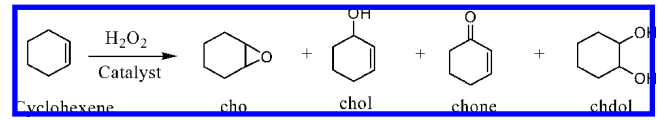

Oxidation of Cyclohexene. Under similar reaction conditions as those used for the oxidation of styrene, we have also carried out the oxidation of cyclohexene. Scheme 3 presents the isolated products. Figure 10 shows the conversion plotted as a function of time, and Table 7 gives details on the product selectivity. Again, a very similar trend was obtained, that is, highest conversion (66%) with complex **7** [$V^{IV}O${sal(chan)}] and lowest (55%) with **8a** [$V^{IV}O${sal(dpen)}]. Moreover, the complexes with the reduced SB ligands show slightly better performance than the complexes with nonreduced SB ligands (salen-type). The main product formed, cyclohexane-1,2-diol, may form from the oxidation of epoxycyclohexane.

Both H_2O_2 and tetrabutylhydroperoxide (TBHP) are known to oxidize cyclohexene in the presence of suitable catalysts. However, under similar conditions, H_2O_2 gives much more efficient epoxidation of cyclohexene. TBHP as an oxidant promotes the allylic oxidation pathway, and epoxidation products only form in low amounts, while with the use of H_2O_2, the oxidation occurs mainly on the double bond and epoxycyclohexane is obtained almost as the sole product. The formation of the allylic-oxidation products cyclohex-2-enone and cyclohex-2-enol reflects the preferential attack of

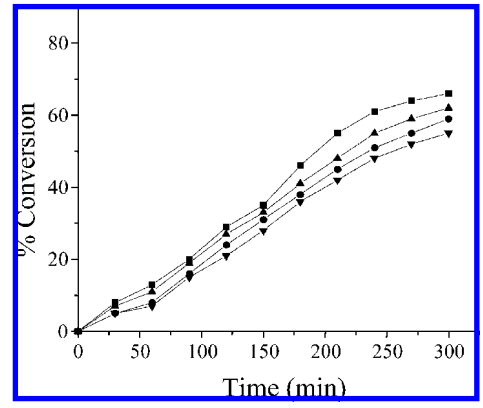

Figure 10. Oxidation of cyclohexene catalyzed by complexes **7** (-■-), **7a** (-▲-), **8** (-●-), and **8a** (-▼-) as a function of time. Reaction conditions: cyclohexene (0.41 g, 5 mmol), catalyst (0.1 mmol), aqueous 30% H_2O_2 (1.13 g, 10 mmol) CH_3CN (10 mL), and temperature (80 °C).

Table 7. Percent Conversion of Cyclohexene, Turnover Frequency (h^{-1}), and Product Selectivity (See Scheme 3)

			selectivity,[a] mol %			
catalyst	conversion (%)	TOF	cho	chdol	chol	chone
$V^{IV}O${sal(chen)} **7a**	62	6.2	9	65	20	6
$V^{IV}O${sal(dpen)} **8a**	55	5.5	5	65	22	8
$V^{IV}O${sal(chan)} **7**	66	6.6	6	76	15	3
$V^{IV}O${sal(dpan)} **8**	59	5.9	8	66	19	7

[a] cho = 1,2-Epoxycyclohexane, chdol = cyclohexane-1,2-diol, chol = cyclohex-2-enol, chone = cyclohex-2-enone. Reaction conditions as mentioned in Figure 10.

Scheme 4. Oxidation Products of Cumene by V−Salen and V−Salan Complexes **7**, **7a**, **8**, and **8a**: Acetophenone (acp), 2-Phenylpropanal (ppa), 1,2-Epoxy-2-phenylpropane (mso), and 2-Phenylpropan-2-ol (ppo)

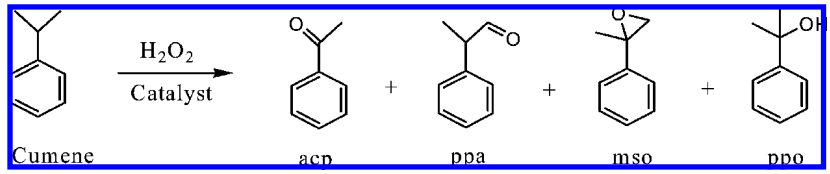

the activated C−H bond over the C=C bond.[61] Valentine and co-workers suggested that the species responsible for the cyclohexene oxidation is the product formed from cleavage of the O−O bond, whereas epoxidation occurs by a direct reaction of the olefin with coordinated HOO^-. Since the O−O bond of HOOH is 5 kcal mol^{-1} stronger than that of TBHP, an HOO^- complex is expected to have a higher activation energy for O−O bond cleavage than a TBHP complex and, therefore, to have a longer lifetime[62] and a higher probability of forming the epoxide.

Oxidation of Cumene. The oxidation of cumene gave acetophenone, 2-phenylpropanal, 1,2-epoxy-2-phenylpropane, and 2-phenylpropan-2-ol (Scheme 4). After several trials, the optimized reaction conditions for the maximum oxidation of 3 mmol of cumene were found to be aqueous 30% H_2O_2 (9 mmol) and acetonitrile (10 mL) at 80 °C, and the results reported concern reactions carried out under these conditions. Figure 11 presents the conversion as a function of time, and Table 8 provides other details.

In general, all complexes exhibit moderate catalytic activities, between 29 and 38%, toward the oxidation of cumene. However, in contrast to other substrates studied here, the conversions of cumene by complexes of salen ligands are 2−6% higher than with the V−salan complexes. Among the various products formed, the selectivity of the important product, acetophenone, is the highest and varies in the range 56−71%.

Oxidation of Tioanisole. The potential of the vanadium complexes as enantioselective catalysts was tested in the asymmetric oxidation with H_2O_2 of a simple model compound, thioanisole.

The reactions were carried out either in CH_2Cl_2 or in 1,2-dichloroethane, as with acetonitrile the stereoselectivity was much lower. Some studies were also carried out in ionic liquids but the enantiomeric excesses were always very low. The results using ionic liquids are presented in the Supporting Information (SI-7). In all cases, the products were only either *R*- or *S*-methyl phenyl sulfoxide, or the sulfone resulting from the oxidation of the sulfoxides. In all tables presented, the percent of sulfone is specified on a molar basis for these three products.

A few control reactions were made to test the noncatalytic oxidation of thioanisole by H_2O_2 in the absence of a catalyst. In section SI-7 (Supporting Information), results of these reactions are presented. While in CH_2Cl_2 or in 1,2-dichloroethane, the conversion was always very low, in some ionic liquids (e.g., butyl methyl pyridinium tetrafluoroborate), the conversion of thioanisole was rather high (77%), but the ee% was zero.

When [V^{IV}O{sal(*S*,*S*-chan)}] (**7**) was used as a representative catalyst, a few reactions were made at $T = 20$ °C varying the concentration and the relative amount of catalyst and its mode of addition (Table 9). At $T = 20$ °C, the conversions were moderate and the enantioselectivities relatively low. The concentration of the catalyst has an influence on the enantioselectivity, higher concentrations leading to lower

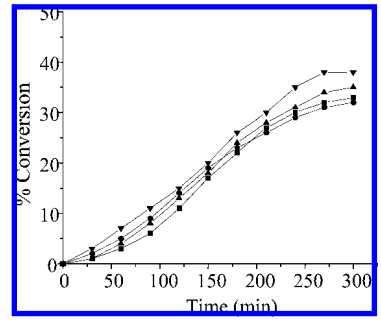

Figure 11. Oxidation of cumene catalyzed by complexes **7** (-■-), **7a**(-▲-), **8** (-●-), and **8a** (-▼-) as a function of time. Reaction conditions: cumene (0.361 g, 3 mmol), aqueous 30% H_2O_2 (1.02, g, 9 mmol), acetonitrile (10 mL), and temperature (80 °C).

Table 8. Percent Conversion of Cumene, Turnover Frequency (h^{-1}), and Product Selectivity (See Scheme 4)

			selectivity,[a] mol %			
catalyst	conversion (%)	TOF	acp	ppa	mso	ppo
V^{IV}O{sal(chen)} **7a**	35	2.1	71	19	12	8
V^{IV}O{sal(dpen)} **8a**	38	2.3	56	23	15	6
V^{IV}O{sal(chan)} **7**	33	2.0	68	25	5	12
V^{IV}O{sal(dpan)} **8**	32	1.9	59	17	10	14

[a] acp = Acetophenone, ppa = 2-phenyl-2-propanal, mso = 1,2-epoxy-2-phenylpropane, ppo = 2-phenylpropan-2-ol. Reaction conditions as mentioned in Figure 11.

Table 9. Sulfoxidation of Thioanisole Using [V^{IV}O{sal(*S*,*S*-chan)}] **7** and [V^{IV}O{sal(*S*,*S*-dpan)}] **8** as Catalysts in Organic Solvents at 20 °C

	mol%		nH_2O_2/		solvent	conv.		%
complex	cat.	[cat] M	*n*S	solvent	(mL)	*t*/h	(%)	ee%[a]	sulfone
7	2.5	0.0084	1.0	MeCN	3	4	81	0	9
7[b]	1.0	0.0009	1.0	CH_2Cl_2	11	4	47	12	5
7[b]	1.0	0.0014	1.2	CH_2Cl_2	7	4	31	15	2
7[b]	1.0	0.005	1.2	CH_2Cl_2	2	2	34	20	3
7[c]	1.0	0.0025	1.2	CH_2Cl_2	4	6	87	21	22
7[c]	1.5	0.0038	1.2	CH_2Cl_2	4	6	88	20	12
7[c]	2.0	0.0050	1.0	CH_2Cl_2	4	6	90	17	11
7[d]	0.75	0.0019	1.2	CH_2Cl_2	4	24	20	7.4	0
7[d]	0.5	0.0013	1.2	CH_2Cl_2	4	24	7	3.2	0
7[d]	0.25	0.001	1.2	CH_2Cl_2	4	24	10	0	0
8[b]	2.5	0.0125	1.0	CH_2Cl_2	2	5	99	8	9
8[b]	2.5	0.0025	1.0	CH_2Cl_2	10	20	48	15	3

[a] The *R*-sulfoxide is preferencially formed when using **7** and the *S*-sulfoxide when using **8**. [b] Slow addition of H_2O_2 in order to try to minimize the formation of sulfone. [c] The aqueous H_2O_2 solution was diluted from 35% to 20%, w/v. [d] The aqueous H_2O_2 solution was diluted from 35% to 15% w/v.

(61) Koola, J. D.; Kochi, J. K. *J. Org. Chem.* **1987**, *52*, 4545–4553.
(62) Nam, W.; Ho, R.; Valentine, J. S. *J. Am. Chem. Soc.* **1991**, *113*, 7052–7054.

Table 10. Sulfoxidation of Thioanisole Using Several V−Salen and V−Salan Complexes As Catalysts in Organic Solvents at 0 °C[a]

complex	nH_2O_2/nS	t/h	conv. (%)	ee %	sulfoxide configuration	% sulfone
$V^{IV}O${sal(*S*,*S*-chan) **7**	1.5	48	44	26	*R*	3
$V^{IV}O${sal(*S*,*S*-chan)} **7**[b]	1.5	18	93	15	*R*	18
$V^{IV}O${mvan(*S*,*S*-chan)} **10**	1.5	18	96	50	*R*	35
$V^{IV}O${mvan(*S*,*S*-chan)} **10**[b]	1.5	18	97	12	*R*	20
$V^{IV}O${sal(*R*,*R*-chen)} **7a**	1.5	19	99	10	*S*	8
$V^{IV}O${sal(*S*,*S*-dpen)} **8a**	1.5	19	>99	26	*S*	45
$V^{IV}O${sal(*S*,*S*-dpan)} **8**	1.5	72	81	1	*S*	19
$V^{IV}O${mvan(*S*,*S*-chen)} **10**	1.5	23	99	14	*R*	32
$V^{IV}O${Etvan(*R*,*R*-chan)} **9**	1.5	24	96	19	*S*	47
$V^{IV}O${Etvan(*R*,*R*-chen)} **9a**	1.5	24	84	0	*S*	16
$V^{IV}O${*t*Busal(*S*,*S*-chan)} **12**	1.5	48	91	14	*S*	30

[a] The reactions were carried out in 4 mL of 1,2-dicloroethane, using a single addition of 1 mol% of catalyst and a single addition of aqueous H_2O_2, 20% (w/v). [b] The reaction was carried out in acetonitrile.

Table 11. Sulfoxidation of Thioanisole Using $V^{IV}O${mvan(*S*,*S*-chan)} **10** as Catalyst in 1,2-Dicloroethane (4 mL) at 0 °C, Making a Single Addition of Aqueous Solution of H_2O_2 20% (w/v)[a]

relative amount of catalyst (mol%)	nH_2O_2/nS	t/h	Conv.(%)	ee%	% sulfone
1	1.5	18	>99	41	27
2.5	1.5	18	95	43	29
5	1.5	18	92	39	24
10	1.5	18	90	38	22
0.5	1.5	48	91	50	28
0.25	1.5	48	0	0	0

[a] The *R*-sulfoxide is the major enantiomer formed.

ee's. Other vanadium complexes were also tested using the experimental conditions where **7** gave better results, but at room temperature, the best ee% observed was ca. 21%. Decreasing the temperature and increasing the reaction time resulted in higher conversion and selectivity. In section SI-8 (Supporting Information), the results obtained at 10 °C are included, and Table 10 shows results at 0 °C.

In all reactions using TBHP as an oxidant, the reactions proceeded much slower than with H_2O_2, and the ee%'s were always very low. The best enantioselectivities were obtained with catalysts $[V^{IV}O${mvan(*S*,*S*-chan)}] (**10**), $[V^{IV}O${sal(*S*,*S*-chan)}] (**7**), and $[V^{IV}O${sal(*S*,*S*-dpen)}] (**8a**).

For catalyst **10**, the effect of the amount of catalyst in the oxidation process was also determined (Table 11). The conversion was ca. 100% with 1 mol% of the catalyst, and the ee was 41%. An increase in the relative amount of catalyst decreased the conversion, but the ee's did not change much. Upon a decrease in the relative amount of the catalyst, the conversion decreased slightly, but the enantioselectivity increased up to 50%. For 0.25% mol%, possibly by action of the oxidant or water, the catalyst decomposed, and no conversion was obtained.

In most cases, a relatively high amount of sulfone was obtained, and in the cases where higher conversions and ee's were obtained, the formation of the sulfone was also higher. This suggests that the ee's obtained are the result of two processes: (i) asymmetric induction in the formation of the sulfoxide and (ii) distinct kinetics of the sulfone formation from the oxidation of the *R*- or *S*-sulfoxide previously formed. In fact, we found that there is a preferential oxidation of one of the enantiomers of the methyl phenyl sulfoxide. Table 12 includes some results of catalytic oxidation studies

Table 12. Oxidation of Racemic Methyl Phenyl Sulfoxide by Several Catalysts at 0 °C[a]

complex	nH_2O_2/nS	t/h	conv. (%)	ee%	nonoxidized sulfoxide configuration	% sulfone
$V^{IV}O${sal(*S*,*S*-chan) **7**	1.5	24	44	9	*R*	44
		48	61	25	*R*	61
$V^{IV}O${mvan(*S*,*S*-chan)} **10**	1.5	24	45	18	*R*	45
		48	65	29	*R*	65
$V^{IV}O${sal(*S*,*S*-dpen)} **8a**	1.5	24	44	6	*S*	44
		48	58	11	*S*	58

[a] The reactions were carried out in 4 mL of 1,2-dicloroethane, using 1 mol% of catalyst and a single addition of aqueous H_2O_2 20% (w/v).

of racemic methyl phenyl sulfoxide to sulfone, giving the data for the ee's of the nonreacted (remaining) methyl phenyl sulfoxide.

The *S*-enantiomer of methyl phenyl sulfoxide is oxidized faster by catalysts **7** and **10** than by the corresponding *R*-enantiomer, and the opposite occurs for **8a**, where an excess of the *R*- enantiomer of methyl phenyl sulfoxide remains after the reaction is stopped. However, the ee's found here for the oxidation of the sulfoxide to sulfone are significantly lower than those obtained in the oxidation of thioanisole to the corresponding sulfoxide.

A previous study[20] reported the asymmetric oxidation of sulfides catalyzed by V−salan systems. The catalyst was formed in situ from the reaction of $VO(acac)_2$ and the chiral ligands. The reported ee%'s were significantly higher than those presented here. However, we were unable to reproduce those results: when doing similar experiments, much lower ee%'s were obtained. Moreover, the preferred enantiomer formed when using complex $[V^{IV}O${sal(*S*,*S*-chan)}] is reported to be the *S*-sulfoxide,[20] while we obtained the *R*-sulfoxide. The recent work of Bryliakov and Talsi[21] also contests the results reported by Sun et al.[20] with lower ee%'s (<20% in most cases) being obtained. Nakajima et al.,[4b] when applying the corresponding V−salen complexes in sulfoxidations with organic peroxides, also obtained the preferred enantiomer of methyl phenyl sulfoxide, in agreement with our results. Moreover, Sun et al.[20] propose a mechanism for sulfoxidation involving V^{IV} complexes and binding of the sulfoxide formed to the vanadium center. As V^{IV}−salan complexes oxidize easily to V^{V} compounds and no evidence was found here for sulfoxide binding to V^{IV} or V^{V} (see below), this proposal also lacks evidence, and the preferred oxidation to sulfone of one of the sulfoxide enantiomers remains to be explained.

Outline of the Mechanisms. Oxidation of Alkenes. Several mechanisms have been proposed for the oxidation of alkenes (e.g., styrene) catalyzed by the vanadium complexes. Outlines of three possible pathways of epoxidation of alkenes catalyzed by V−salan complexes[63,64] are depicted in Scheme 5. The epoxides formed may experience further oxidation, but we will not present any study for these processes.

(63) Deubel, D. V.; Frenking, G.; Gisdakis, P.; Herrmann, W. A.; Rösch, N.; Sundermeyer, J. *Acc. Chem. Res.* **2004**, *37*, 645–652.
(64) Kala Raj, N. K.; Ramaswamy, A. V.; Manikandan, P. *J. Mol. Catal. A: Chem.* **2005**, *227*, 37–45.

Scheme 5. Outlines of Plausible Mechanisms of Alkene Epoxidation Catalysed by the V^{IV}−Salan Complexes (See Text)[a]

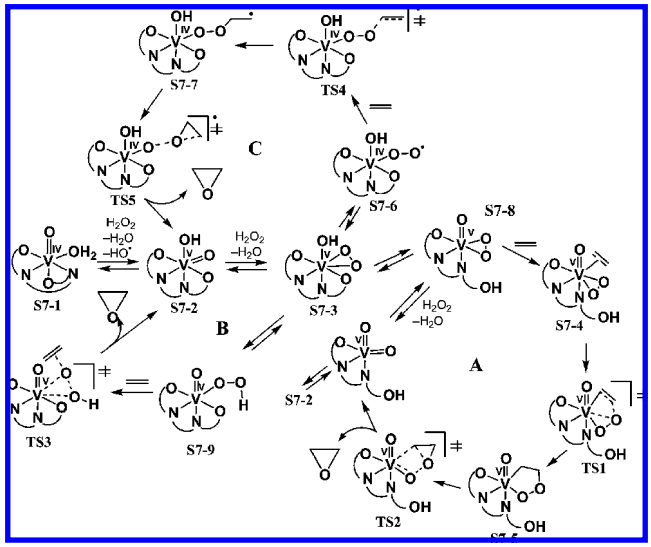

[a] A separate numbering of the structures is used in this scheme for the model complexes starting with **S7**-, and for the calculated transition states starting with **TS**-.

To elucidate which of these epoxidation mechanisms is the most favorable one, we performed preliminary quantum-chemical calculations for the model complexes with the ligand L being $\{CH_2-NH-CH_2-CH=CH-O^-\}_2$ instead of the salan ligands tested in this work. In these studies, we are also considering the alkenes as simply ethylene. We should emphasize that, for each structure presented in Scheme 5, several isomers are possible. Meanwhile, the calculations were carried out only for the isomers in which two O atoms and one N atom of L occupy equatorial positions and another N atom of L is in the axial position. Namely, this isomeric form was found to be the most stable for the vanadium dioxo-N,N′-ethylenebis-(pyridoxylaminato) complexes on the basis of theoretical and experimental X-ray structural data.[7,8] The calculations taking into account other possible isomeric forms are continuing, and when complete, the results will be presented in a separate publication.

In the first step of the reaction, the starting V^{IV} complex **S7-1** is oxidized by H_2O_2 to V^V complex **S7-2**, the active species of the catalyst, which reacts further with the oxidant to form peroxo complexes **S7-3**. Both these reactions are well-known in vanadium chemistry, and the corresponding mechanisms were considered previously by Shul'pin et al.[65] and by Khaliullin et al.[66] The next stage involves an epoxidation of the C=C double bond of the alkene by the peroxo ligand of **S7-3**, and for this process, three routes are considered.

The first, Mimoun-type mechanism[67] (part **A** in Scheme 5) involves the coordination of an alkene molecule to the metal, followed by the formation of a peroxometallocyclic intermediate **S7-5**, which decomposes into epoxide and catalyst **S7-2** or **S7-8**. For this mechanism, the generation of intermediates **S7-4** and **S7-5** and transition state **TS1** requires the cleavage of one of the V−*N*,*O*−ligand bonds to liberate one coordination position. It was shown[66] that in vanadium complexes with N,O-ligands such as pca (Hpca = pyrazine-2-carboxylic acid) the oxygen atom of pca undergoes protonation instead of the nitrogen atom. Hence, it may be assumed that the proton migration from the OH ligand to an oxygen of the salan ligand and cleavage of the V−O bond is the step preceding the reaction with alkene and the formation of **TS1**.

The calculations revealed that transition state **TS1** with the O atoms of both L and alkylperoxo ligands being in the trans position is more stable (by 1.9 kcal mol^{-1}) than **TS1′** with the O atoms in cis position (Figure 12). The apparent activation energy (E_a^{ap}) for **TS1** relative to complex **S7-3** is 32.7 kcal mol^{-1}.

Within the second, Sharpless-type mechanism,[68] (part **B** in Scheme 5), the epoxidation is considered as a concerted one-step process where a direct attack of the alkene on the peroxo ligand occurs. Reaction may start either from the hydroxo species **S7-3** or from the hydroperoxo complex **S7-9** derived from **S7-3** upon a proton migration. The calculations indicate that the second pathway is more energetically favorable (by 2.9 kcal mol^{-1}) compared with the first one. Two transition states (**TS3** and **TS3′**) corresponding to the "rear" and "front" attack of the hydroperoxo ligand in **S7-9** have virtually the same energy (the difference is only 0.3 kcal mol^{-1}). The calculated E_a^{ap} value for **TS3** relative to **S7-3** is 24.5 kcal mol^{-1}, which is significantly lower than that for the Mimoun mechanism.

The third plausible mechanism was examined by Manikandan et al.[64] and is based on the generation of the diradical V−peroxo complex **S7-6** followed by an attack of the alkene and formation of the diradical alkylperoxo intermediate **S7-7** (part **C** in Scheme 5). The second step of this mechanism (via **TS5**) is found to be rate-limiting since **TS5** is by 3.0 kcal mol^{-1} higher in energy than **TS4**. The apparent activation energy for **TS5** relative to complex **S7-3** is 26.4 kcal mol^{-1}, 1.9 kcal mol^{-1} higher than the activation barrier for the Sharpless mechanism. Thus, the theoretical calculations suggest that the Sharpless-type mechanism of alkene epoxidation involving the hydroperoxo species **S7-9** is the most favorable one.

In order to study how the simplification introduced with the ligand model affects the energetic features of the epoxidation, the key structures with ligand L = $\{CH_2NHCH_2-(o-C_6H_4O^-)\}_2$ (**S7-3ph**, **TS3ph**, and **TS5ph**, Figure 12) for two of the most plausible routes, that is, Sharpless mechanism (**B**) and biradical mechanism (**C**), were calculated. The results indicate that (i) the activation barrier of the Sharpless mechanism increases only slightly (by 0.6 kcal mol^{-1}) upon a change of the model, whereas the barrier of the biradical pathway is not changed at all, and (ii) the Sharpless

(65) Shul'pin, G. B.; Kozlov, Y. N.; Nizova, G. V.; Süss-Fink, G.; Stanislas, S.; Kitaygorodskiy, A.; Kulikova, V. S. *J. Chem. Soc., Perkin Trans. 2* **2001**, 1351–1371.
(66) Khaliullin, R. Z.; Bell, A. T.; Head-Gordon, M. *J. Phys. Chem. B* **2005**, *109*, 17984–17992.
(67) Mimoun, H.; Seree de Roch, I.; Sajus, L. *Tetrahedron* **1970**, *26*, 37–50.
(68) Sharpless, K. B.; Townsend, J. M.; Williams, D. R. *J. Am. Chem. Soc.* **1972**, *94*, 295–296.

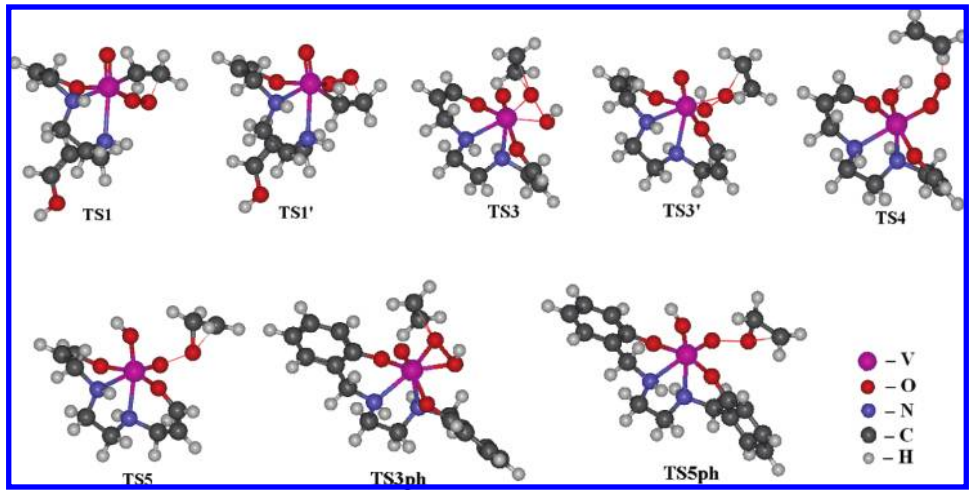

Figure 12. Equilibrium geometries of the calculated transition states included in Scheme 5.

mechanism remains the most favorable. More detailed theoretical mechanistic studies of olefin epoxidation catalyzed by vanadium complexes with reduced Schiff base N,O ligands are in progress.

It is interesting to remark that the complex $[V^{IV}O(L)(C_2H_4)]$ (**S8-1**) could be refined in our DFT calculations (with rather long V−C distances of 2.649 and 2.667 Å); however, its energy is by 11.0 kcal mol^{-1} higher than the similar water adduct **S7-1**. This corroborates the fact that the corresponding species of **S8-1** $[V^{IV}O\{sal(chan)(styrene)\}]$ were never detected in EPR experiments with solutions of $[V^{IV}O\{sal(chan)\}]$ (**7**), even when using a 50−100 fold excess of styrene. The corresponding $[V^{V}O\{sal(chan)(styrene)\}]$ adduct (one isomer corresponds to **S7-4**) was also never detected in oxidized solutions of **7**, upon adding a 50−100-fold excess of styrene, either in the presence or absence of H_2O_2. The only additional peaks found in these solutions were at −580 ppm, detected in methanolic solutions, which correspond to $[V^{V}O(O_2)\{sal(chan)\}]$ species, and the diperoxovanadate (at −648 ppm).

In our preliminary calculations with the model system, structures such as **S8-2** with the protonated or non-protonated bidentate peroxo ligand were never obtained, but instead the calculations converged to structures such as **S7-9** (Scheme 6) or **S7-8**, respectively.

Oxidation of Thioanisole. As far as the mechanism of oxidation of thioanisole is concerned, no DFT calculations were carried out so far by our group. When ^{51}V NMR was used, no additional peaks were found in oxidized solutions of **7**, adding an excess of thioanisole in the presence or absence of H_2O_2. We anticipate that a mechanism similar to that outlined by Pecoraro and co-workers[69] is operating, that is, the formation of an intermediate such as **S8-2** (or **S7-9**), that may form from species **S7-3** or not involve such a protonated oxo moiety. Interaction of the thioether with the coordinated hydroperoxo moiety may lead to the sulfoxide.[69]

It has been reported that, in salan complexes, there is the possibility of hydrogen bonding of the N−H hydrogen and

Scheme 6. Examples of Calculated Structures for $[V^{IV}O(L)(C_2H_4)]$ and $[V^{V}O(L)\underline{O}OH]$[a]

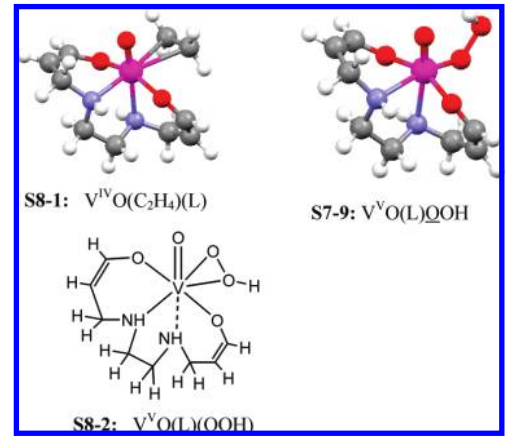

[a] In the preliminary calculations carried out for structures such as **S8-2** (complexes with the bidentate hydroperoxo ligand), the optimizations always converged to species where either L is tridentate or the peroxide becomes monodentate (e.g. **S7-9**).

the coordinated peroxo group, and that this has a crucial role in the catalytic process.[21] In the present work, no particular effect was found as far as conversion is concerned. For the enantioselectivity, further experimental and computational studies are required to understand the factors that may be relevant for determining the success of the asymmetric sulfoxidations.

Conclusions

Several chiral salen and salan compounds and the corresponding V^{IV}−salen and V^{IV}−salan complexes were synthesized and characterized. Namely, the crystal and molecular structures of $H_2sal(R,R\text{-chan})^{2+}\cdot 2Cl^{-}\cdot(CH_3)_2CHOH\cdot H_2O$ (**1c**), Etvan(*S*,*S*-chen) (**3c**), and naph(*R*,*R*-chen) (**6c**) were solved by X-ray diffraction methods, which show the higher flexibility of the reduced Schiff base ligand sal(*R*,*R*-chan), when compared to naph(*R*,*R*-chen) or Etvan(*S*,*S*-chen). The CD spectra of the salan ligands and V^{IV}−salan complexes are less intense than those of the corresponding salen compounds.

(69) Schneider, C. J.; Penner-Hahn, J. E.; Pecoraro, V. L. *J. Am. Chem. Soc.* **2008**, *130*, 2712–2713.

In the solid state, the V^{IV}−salan compounds are monomeric, but as judged by the ν(V=O) stretching frequencies, significant V^{IV}=O····V^{IV}=O interactions are operating. Upon being dissolved in common organic solvents such as methanol or acetonitrile in the presence of air, the V^{IV}−salan compounds oxidize easily. The oxidation process was followed using spectroscopic techniques (EPR, UV−vis, ^{51}V NMR), [$V^{V}O_2$(salan)] and [V^{V}O(salan)(CH_3OH)] species being formed. From these solutions, solids were obtained which were found to be composed of dinuclear OV^{V}(μ-O)-V^{V}O species with binding modes involving the four donor atoms of the ligands and the μ-oxo bridge. The crystal and molecular structures of [{V^{V}O[sal(*S*,*S*-dpan)]}$_2$(μ-O)]·H_2O·2$(CH_3)_2$CHOH} (**14c**) and [{V^{V}O[*t*-Busal(*R*,*R*-chan)]}$_2$-(μ-O)]·2$(CH_3)_2$CHOH (**15c**) were also determined by single-crystal X-ray diffraction, these two compounds being the first examples of dinuclear complexes with tetradentate ligands with the $V^{V}_2O_3^{4+}$ core.

The V^{IV}−salan complexes **7**, **7a**, **8**, and **8a**, applied as catalysts in the oxidation of styrene and cyclohexene by hydrogen peroxide, showed 52−71% conversion in 5 h with turnover frequencies of 5.2−7.1 h^{-1}. Although most complexes did not show very good selectivity, the salan complexes normally presented slightly better performance in the oxidation of styrene and cyclohexene than the salen derivatives, and within the two types of complexes, the chan/chen derivatives are better than dpan/dpen ones. Among the various oxidized products of styrene formed, the selectivity for benzaldehyde is highest. Similarly, the selectivity for cyclohexane-1,2-diol is highest among the various oxidation products of cyclohexene. The percentage conversion of cumene with these complexes is only 32−38% with turnover frequencies of 1.9−2.3 h^{-1}, and acetophenone was the product obtained in the highest yield.

The V−salen and V−salan complexes were also applied as catalysts in the sulfoxidation of thioanisole by hydrogen peroxide and showed high activities and moderate enantioselectivity for this process. Various parameters were tested, such as solvent, temperature, catalyst loading, catalyst concentration, and phenolic ring substituent effects on overall conversion and enantioselectivity. Methoxy substituents adjacent to the phenolate group improve chiral induction. Lower temperatures also have a positive effect on enantioselectivity. The catalyst concentration also required optimization. Catalyst loadings higher or lower than 1 mol % slow down the catalytic reaction and decrease enantioselectivity. Part of the enantioselectivity in the sulfoxidations is originated by kinetic resolution in the oxidation of the *R*- and *S*-sulfoxides formed. For example, the *S*-methylphenylsulfoxide is oxidized faster to sulfone by catalysts **7** and **10**, than the corresponding *R*-enantiomer, and the opposite occurs for **8a**, where an excess of *R*-methylphenylsulfoxide remains after the reaction is stopped.

Preliminary DFT calculations were carried out with a model system to understand which is the most favorable mechanism in alkene epoxidation, and as far as we know, a theoretical comparison of the several alternative mechanisms for epoxidation has not been reported previously. The calculations suggest that a simple bimolecular mechanism where the nucleophile and the hydroperoxo−metal complex react, that is, a Sharpless-type mechanism, is the most favorable one, although the radical route, with a reaction pathway involving the generation of a diradical alkylperoxo intermediate, should also be competitive.

In solutions of organic solvents containing water, the V^{IV}−salan complexes are much less susceptible to hydrolysis than the corresponding the V^{IV}−salen compounds. Moreover, upon the addition of aqueous H_2O_2, the relative amount of inorganic peroxovanadates is significantly lower in the case of the V^{V}−salan compounds.

Globally, the V^{IV}−salan compounds appear to be more promising for catalytic oxidations than their V^{IV}−salen counterparts. The much higher hydrolytical stability of V^{IV}− and V^{V}−salan as compared with their corresponding V^{IV}− and V^{V}−salen compounds indicates that the M−salan complexes may be promising in procedures where the recyclability is an important issue. Attempts to prepare immobilized catalysts with these systems are presently being carried out.

Acknowledgment. The authors wish to thank the Portuguese NMR Network (IST-UTL Center) for providing access to the NMR facility and the National Mass Spectroscopy Network (RNEM) and Dr. Maria da Conceição Oliveira for the ESI-MS measurements. M.R.M. acknowledges the Department of Science and Technology, Government of India for financial support. POCI 2010, FEDER, Fundação para a Ciência e Tecnologia (SFRH/BPD/13975/2003 and SFRH/BD/40279/2007), PPCDT/QUI/55985/2004, and PPCDT/QUI/56949/2004 are acknowledged for financial support.

Supporting Information Available: Additional data for the ligands and complexes synthesized; additional X-ray data for compounds **1c**, **3c**, **14c**, and **15c**; magnetic properties; circular dichroism spectra; Kamlet-Taft LSER; additional ^{51}V NMR data; sulfoxidations using ionic liquids; sulfoxidations at 10 °C; DFT calculations; and additional documentation of the single-crystal X-ray structures. This material is available free of charge via the Internet at http://pubs.acs.org.

IC8017985